The Meteoritical Society

Meteoritics & Planetary Science 49, Nr 2, 261–291 (2014)
doi: 10.1111/maps.12239

The origin of young mare basalts inferred from lunar meteorites Northwest Africa 4734, 032, and LaPaz Icefield 02205

Stephen M. ELARDO[1*], Charles K. SHEARER Jr.[1], Amy L. FAGAN[2,3], Lars E. BORG[4], Amy M. GAFFNEY[4], Paul V. BURGER[1], Clive R. NEAL[2], Vera A. FERNANDES[5], and Francis M. McCUBBIN[1]

[1]Department of Earth & Planetary Sciences, Institute of Meteoritics, University of New Mexico, Albuquerque, New Mexico 87131, USA
[2]Department of Civil & Environmental Engineering & Earth Sciences, University of Notre Dame, Notre Dame, Indiana 46556, USA
[3]Lunar & Planetary Institute, USRA, Houston, Texas 77058, USA
[4]Chemical Sciences Division, Lawrence Livermore National Laboratory, Livermore, California 94550, USA
[5]Museum für Naturkunde- Berlin, Leibniz-Institut für Evolutions- und Biodiversitätsforschung, Invalidenstrasse 43, 10115 Berlin, Germany
[*]Corresponding author. E-mail: selardo@unm.edu

(Received 23 January 2013; revision accepted 21 October 2013)

Abstract–Northwest Africa (NWA) 4734 is an unbrecciated basaltic lunar meteorite that is nearly identical in chemical composition to basaltic lunar meteorites NWA 032 and LaPaz Icefield (LAP) 02205. We have conducted a geochemical, petrologic, mineralogic, and Sm-Nd, Rb-Sr, and Ar-Ar isotopic study of these meteorites to constrain their petrologic relationships and the origin of young mare basalts. NWA 4734 is a low-Ti mare basalt with a low Mg* (36.5) and elevated abundances of incompatible trace elements (e.g., 2.00 ppm Th). The Sm-Nd isotope system dates NWA 4734 with an isochron age of 3024 ± 27 Ma, an initial ε_{Nd} of +0.88 ± 0.20, and a source region $^{147}Sm/^{144}Nd$ of 0.201 ± 0.001. The crystallization age of NWA 4734 is concordant with those of LAP 02205 and NWA 032. NWA 4734 and LAP 02205 have very similar bulk compositions, mineral compositions, textures, and ages. Their source region $^{147}Sm/^{144}Nd$ values indicate that they are derived from similar, but distinct, source materials. They probably do not sample the same lava flow, but rather are similarly sourced, but isotopically distinct, lavas that probably originate from the same volcanic complex. They may have experienced slightly different assimilation histories in route to eruption, but can be source-crater paired. NWA 032 remains enigmatic, as its source region $^{147}Sm/^{144}Nd$ definitively precludes a simple relationship with NWA 4734 and LAP 02205, despite a similar bulk composition. Their high Ti/Sm, low $(La/Yb)_N$, and Cl-poor apatite compositions rule out the direct involvement of KREEP. Rather, they are consistent with low-degree partial melting of late-formed LMO cumulates, and indicate that the geochemical characteristics attributed to urKREEP are not unique to that reservoir. These and other basaltic meteorites indicate that the youngest mare basalts originate from multiple sources, and suggest that KREEP is not a prerequisite for the most recent known melting in the Moon.

INTRODUCTION

To date, there are ten recognized unbrecciated mare basaltic lunar meteorites (e.g., Korotev 2005; Greshake et al. 2008; Joy et al. 2008; Haloda et al. 2009). All are classified as low- or very low-Ti mare basalts (Neal and Taylor 1992). The lack of high-Ti basalts in the meteorite suite is not surprising, given that interpretation of orbital data sets indicates that basaltic units with >5 wt% TiO_2 compose only approximately 20% of lunar maria (Giguere et al. 2000; Gillis et al. 2003; Lucey et al. 2006), and that low-Ti magmatism

© The Meteoritical Society, 2014.

represents the vast majority of mare magmatism that occurred over more than 1 Gyr of lunar history (Nyquist and Shih 1992; Shearer and Papike 1999; Snyder et al. 2000; Hiesinger et al. 2003; Shearer et al. 2006). From an isotopic and trace element perspective, the source regions for the basaltic lunar meteorites span a greater compositional range than the Apollo low-Ti basalts, and are from both the most incompatible trace element (ITE)-depleted source regions, yet recognized on the Moon (Misawa et al. 1993; Nyquist et al. 2007; Gaffney et al. 2008), to some of the most ITE-enriched (Jolliff et al. 2003; Borg et al. 2004, 2009). Given that lunar meteorites should provide a generally random sampling of the lunar surface (Korotev et al. 2003; Korotev 2005; Warren 2005), these ten basaltic lunar meteorites, plus the basaltic lithology within Kalahari 009, have essentially doubled the number of mare basalt units in the lunar sample collection. When considering that the ages of basaltic lunar meteorites alone span approximately 1.4 billion years of mare magmatism (e.g., Misawa et al. 1993; Nyquist et al. 2007; Terada et al. 2007; Shih et al. 2008; Sokol et al. 2008; Fernandes et al. 2009a; Haloda et al. 2009) and include the youngest lunar igneous samples yet dated, these samples significantly add to our knowledge about compositional diversity and magma production within the lunar mantle.

Although there is some evidence that mare magmatism on the lunar nearside persisted until approximately 1.0–1.2 Ga (Hiesinger et al. 2000, 2003, 2010), the youngest dated mare basalt is currently the paired stones Northwest Africa (NWA) 032 and 479, with an age of 2931 ± 92 Ma (Borg et al. 2009). The mare basaltic meteorites LaPaz Icefield (LAP) 02205 and its pairings (2991 ± 14 Ma; Rankenburg et al. 2007), NWA 773 (2993 ± 32 Ma; Borg et al. 2009) and Northeast Africa (NEA) 003A (3089 ± 64 Ma; Haloda et al. 2009) produce similarly young and overlapping ages. In addition, the source region Sm/Nd for these meteorites indicates that magma production was occurring in some of the most ITE-depleted (NWA 032) mantle source regions on the Moon simultaneously with some of the most enriched (NWA 773). It has been suggested that heat production from KREEP (the potassium-, rare earth element–, and phosphorus-rich lunar magma ocean residuum) reservoirs in the mantle may be required to produce partial melts after the lunar interior had extensively cooled (Warren and Wasson 1979; Wieczorek and Phillips 2000; Hess and Parmentier 2001; Borg et al. 2004); however, the diversity in source region composition between contemporaneous low-Ti mare basalts indicates that melting at approximately 3 Ga involved several distinct source regions and heat sources.

Adding an even greater degree of complexity to the origin of young mare basalts, three samples, in particular, have intriguing geochemical features. NWA 032/479 and LAP 02205 have nearly indistinguishable bulk-rock major and trace element compositions, mineral major element compositions, and ages (Fagan et al. 2002; Barrat et al. 2005; Righter et al. 2005; Zeigler et al. 2005; Anand et al. 2006; Day et al. 2006; Joy et al. 2006; Rankenburg et al. 2007; Borg et al. 2009; Hill et al. 2009); consequently, they have been suggested to be source-crater paired (e.g., Zeigler et al. 2005). However, their isotopic compositions strongly suggest that NWA 032 is derived from a source region that is significantly more LREE-depleted than LAP 02205. Furthermore, a third sample found in Morocco in 2001, NWA 4734, is texturally and geochemically similar to the LAP suite of meteorites (Connolly et al. 2008; Fernandes et al. 2009b; Korotev et al. 2009; Wang et al. 2012). Together, these three basalts are some of the most ITE-enriched low-Ti mare basalts yet found, with deep negative Eu anomalies as well as REE and Th abundances 2–3 times greater than Apollo 12 and 15 low-Ti basalts.

In this work, we present a detailed petrologic, mineralogic, geochemical, and isotopic study of NWA 4734, NWA 032, and LAP 02205 to place better constraints on their origin and to address some of the questions they raise. Do these three meteorites sample the same basaltic unit, or are they derived from different mantle source regions? Can the significantly more depleted source region $^{147}Sm/^{144}Nd$ for NWA 032 be reconciled with its strong compositional and mineralogic similarities to LAP 02205 and NWA 4734? Is KREEP necessary to produce their incompatible trace element enrichment and heat for melting? What is the role of KREEP in the production of young mare basalts, and what is the diversity in source regions being melted near the end of mare magmatism?

ANALYTICAL METHODS

Electron Probe Microanalysis and Secondary Ion Mass Spectrometry

We examined three sections of NWA 4734, two sections of NWA 032, and LAP 02205,30 and LAP 02224,7 (collectively referred to hereafter as LAP). The LAP samples, along with four additional basaltic lunar meteorites from the LaPaz Icefield, are identical in composition and considered paired (Zeigler et al. 2005; Hill et al. 2009). Samples of NWA 032 and 4734 belong to the meteorite collection at the Institute of Meteoritics, University of New Mexico (UNM), and the thin sections of LAP were allocated to us by the

Meteorite Working Group, NASA Johnson Space Center. Mineral analyses and wavelength-dispersive spectrometry (WDS) mapping were conducted on mineral phases in all three meteorites. Each sample was documented via backscattered electron (BSE) imaging to understand textural relationships before quantitative analyses were conducted. Quantitative WDS analyses were conducted on olivine, pyroxene, Cr-Fe-Ti-oxides, plagioclase, and phosphates using the JEOL JXA 8200 electron microprobe (EMP) housed in the Institute of Meteoritics, UNM. Minor phases were identified using energy-dispersive spectrometry (EDS). Quantitative WDS analyses were conducted using an accelerating voltage of 15 kV, a beam current of 30 nA, and a 1 μm spot size for all phases except plagioclase, which was analyzed with a 20 nA beam current and 5 μm spot size to minimize Na volatilization. Phosphates were analyzed with a 20 nA beam current and 1–3 μm spot size according to the methods outlined by McCubbin et al. (2010a, 2010b, 2011), and were monitored for variable F X-ray count rates (e.g., Stormer et al. 1993; Pyle et al. 2002; Goldoff et al. 2012) using the JEOL real-time chart recorder. Apatite analyses showing variable F count rates were discarded. Standards were a mix of both natural and synthetic minerals and oxides, and the quality of analyses were assessed based on stoichiometric constraints. Qualitative K_α X-ray maps of Mg, Ti, Al, Ca, and Cr in pyroxene grains in LAP, NWA 4734, and NWA 032 were made to compare zoning patterns. Maps were made using the same instrument operating at 15 kV and 100 nA, with dwell times of 120–180 ms, and a 1 μm pixel size. In addition, qualitative K_α X-ray maps of Si, Ti, Al, Cr, Fe, Mg, Ca, K, P, and S were made at 15 kV and 100 nA with a dwell time of 25 ms and a pixel size of 4 μm over a 24 mm^2 area of NWA 4734 (Fig. 1a; the majority of a section) to illustrate phase distributions and determine modal abundances. Phase abundances were determined using the program PhaseQuant (Elangovan et al. 2012) by subtracting void space before normalizing mineral abundances to 100%.

Secondary ion mass spectrometry (SIMS) analyses of Ni and Co in olivine were conducted using the Cameca ims 4f ion microprobe housed in the Institute of Meteoritics, UNM, using similar operating conditions as Shearer and Papike (2005), Borg et al. (2009), and Elardo et al. (2011). A primary O^- ion beam was accelerated through a nominal potential of 10 kV. A 15 nA beam current was used, resulting in a spot size of approximately 15–20 μm. Sputtered secondary ions were energy-filtered using a sample offset voltage of 105 V. Absolute elemental concentrations were calculated using empirical relationships of trace element/$^{30}Si^+$ ratios (normalized to known SiO_2) to element concentrations derived from calibration curves.

Bulk-Rock Chemical Analyses

Bulk-rock compositional analyses of major, minor, and trace elements in NWA 4734 were conducted at the University of Notre Dame. The aliquot of NWA 4734 (0.0586 g) was hand-ground with an agate mortar and pestle in a class 1000 clean laboratory before being digested in twice-distilled HNO_3 and 29N HF in a ratio of 1:2 before being brought to a final volume of 100.04 g in 1.0 N (approximately 5%) HNO_3. This procedure was also followed for procedural blanks and standard reference materials, which were analyzed in conjunction with NWA 4734.

Major element analyses were quantified by solution-mode using a Perkin Elmer 3300 XL Optima Inductively Coupled Plasma-Optical Emission Spectrometer (ICP-OES) located at the Center for Environmental Science and Technology at the University of Notre Dame. All major and minor elements were determined, except SiO_2, because the samples were prepared by hydrofluoric acid dissolution, making Si volatile (as tetrafluoride) during the dissolution process; SiO_2 was calculated, therefore, by subtracting the wt% of the other oxides, including trace elements, from 100%. Instrument sensitivity was calibrated to six calibration solutions (including a blank), which were made with known concentrations of all analyzed elements to ideally bracket the abundance of each element in the unknown samples. A calibration solution was used as the drift-correction solution and blank solutions (5% HNO_3) were measured throughout the analysis. NWA 4734, procedural blanks, and the standard reference materials (BIR1a, BHVO-1, BHVO-2, BCR-2) were analyzed as "unknown" materials. NWA 4734 was analyzed in duplicate, where each analysis is the arithmetic mean of three separate measurements by the instrument. The data were reduced using the USGS basalt standard reference material BIR-1 (Flanagan 1984; Gladney and Roelandts 1988; Govindaraju 1994) following the method of Mahoney et al. (2001).

Trace elements were quantified using solution-mode ICP-mass spectrometry with the Thermo-Finnigan Element 2 ICP-MS instrument at the Midwest Isotope and Trace Element Research and Analytical Center (MITERAC) housed at the University of Notre Dame. The protocol of Neal (2001) modified from Jenner et al. (1990) was followed. Procedural blanks and USGS basaltic standard reference materials were analyzed as unknowns. Two standard solutions were analyzed and used during the data reduction process. Two washes of 5% and 10% HNO_3 were performed between each analysis, including standards, blanks, and unknowns.

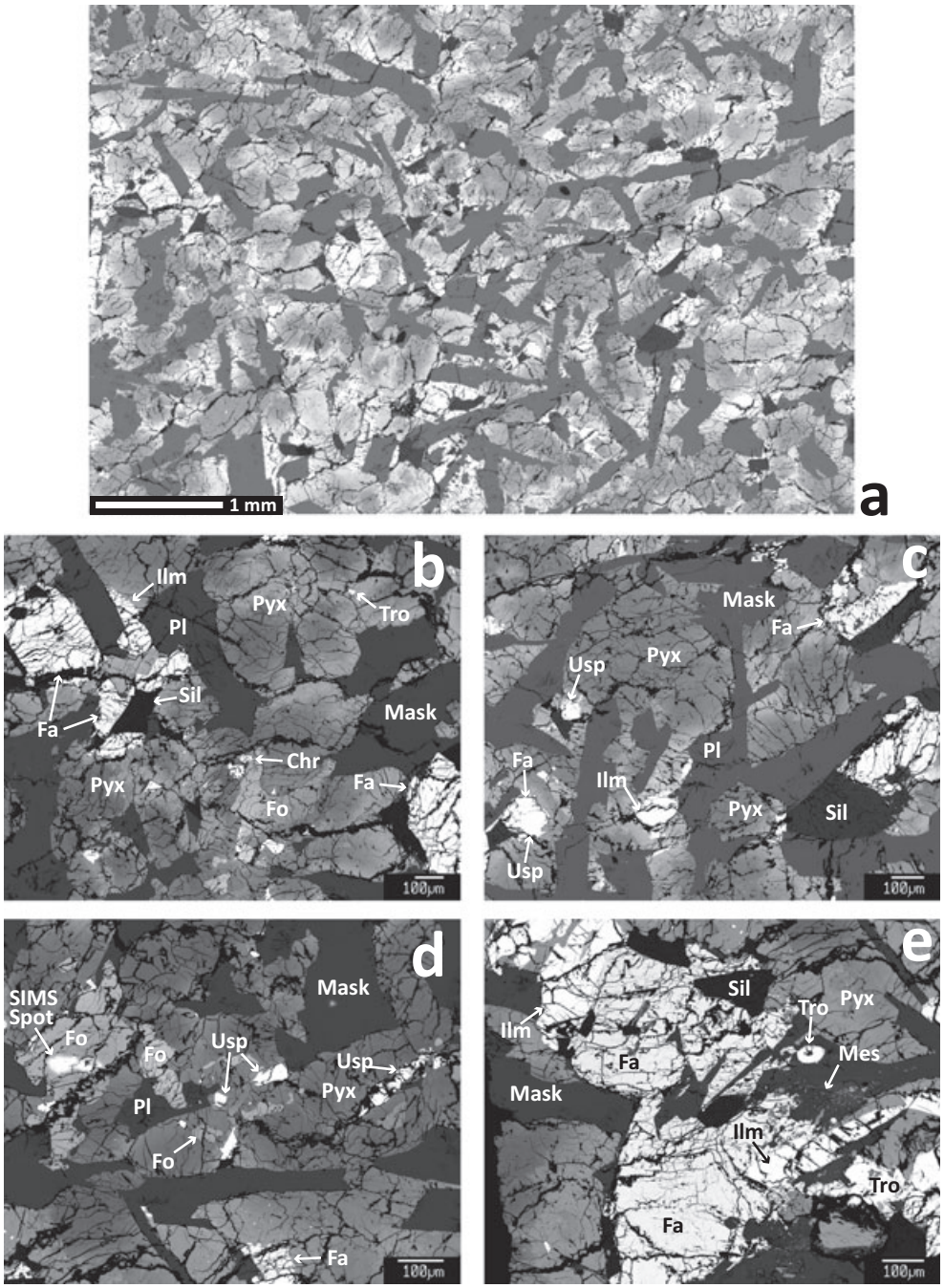


Fig. 1. Backscattered electron (BSE) images of NWA 4734. a) The 4 × 6 mm area of NWA 4734 from which modal abundances were determined from corresponding WDS maps. b–e) Representative areas of NWA 4734 showing phases and typical textural occurrences.

Rb-Sr and Sm-Nd Isotopic Analyses

Rb-Sr and Sm-Nd isotopic analyses were completed on two separate chips of NWA 4734. The separation procedure is presented in Fig. S1. Mineral separates and the first whole rock (Wr-1) were derived from the first approximately 0.5 g chip obtained from Anthony Irving at the University of Washington. Another approximately 0.5 g chip was obtained from the meteorite collection at the Institute of Meteoritics, UNM, and used for Sm-Nd isotopic analysis of a second whole rock (Wr-2), as well as for determination of the Sm isotopic composition (IC) of NWA 4734. Mineral separates were obtained by gently crushing the

first chip in a sapphire mortar and pestle and sieving at 150 μm (100 mesh), 75 μm (200 mesh), and 44 μm (325 mesh) size fractions. The 75–150 μm and 44–75 μm size fractions were processed through a Frantz isodynamic separator yielding plagioclase-rich (nonmagnetic at 0.45 amperes), Fe-pyroxene-rich (magnetic at 0.20 amperes), and Mg-pyroxene-rich (magnetic at 0.45 amperes) mineral fractions. These fractions were then hand-picked in ultrapure alcohol to remove obvious impurities, such as sieve fibers. Composite grains made up of plagioclase, pyroxene, and oxides were not separated. Nevertheless, the fractions were >95% pure after separations were completed. Prior to digestion, the magnetic fractions from both 75–150 μm and 44–75 μm sieve fractions were combined.

Following the procedure developed for NWA 032 (Borg et al. 2009), the Wr-1 fraction was leached in 2N HCl at 25 °C for 10 min in an ultrasonic bath and in 4N HCl on a hot plate for 15 min at 45 °C, yielding the residue (Wr-1R), the 2N HCl leachate (Wr-1 2L), and 4N HCl leachate (Wr-1 4L) fractions. Isotopic analysis of the leachate and residue fractions demonstrated that only the 2N HCl leachate was contaminated by Sm and Nd derived from the desert environment. As a consequence, the mineral fractions were leached in 2N HCl for 10 min in an ultrasonic bath at 25 °C. The second chip was processed similarly, except that the initial leaching was completed in 0.5M acetic acid and final leaching was completed in 1N HCl in an ultrasonic bath at 25 °C for 10 min each. Rb-Sr and REEs were separated using cation exchange columns filled with BioRad AG-50 × 8 200–400 mesh resin in 2N HCL, 2N HNO_3, and 6N HCl. The REEs were purified using Eichrom RE-spec resin in 0.05N and 1N HNO_3 prior to loading on pressurized 2-hydroxyisobutyric acid columns. The 2-hydroxyisobutyric acid was separated from the Sm and Nd using 2 mL cation clean-up columns. Total procedural blanks include contributions associated with digestion, isotopic tracers, and ion exchange columns, and were Rb = 8.5 pg, Sr = 23 pg, Sm = 5.8 pg, and Nd = 17 pg. Rb and Sr were separated from the 4N HCl leachate using Eichrom Sr-Spec resin in 3N HNO_3 and water. Rb and Sr blanks associated with this column are 2 and 49 pg, respectively.

Sm and Nd isotopic analyses were completed using the Thermo Scientific TRITON thermal ionization mass spectrometer at Lawrence Livermore National Laboratory. Fractions were run as Nd^+ and Sm^+ in static mode on 18–513 ng of Nd and 6–214 ng of Sm using a double zone refined Re filament configuration. Nd was corrected for fractionation assuming $^{146}Nd/^{144}Nd = 0.7219$, whereas Sm was corrected assuming $^{147}Sm/^{152}Sm = 0.56083$. Potential interfering elements were monitored, but were trivial and resulted in corrections that were significantly smaller than the uncertainty associated with individual mass spectrometry runs. The sizes of the Sm and Nd ion beams were highly variable as a result of the vastly different amounts of these elements in the mineral fractions. The ^{144}Nd beam varied from 5E-12 to 5E-11 amperes, and the ^{152}Sm ion beam varied from 1E-12 to 5E-12 amperes. Rb and Sr were loaded on a single zone refined Re filaments in 2N HCl with a 99.999% pure Ta_2O_5 emitter and run on the TRITON in static mode. Sr was corrected for instrument mass fractionation assuming $^{86}Sr/^{88}Sr = 0.1194$, whereas Rb was corrected by comparing values obtained on NBS-984 Rb standard to $^{85}Rb/^{87}Rb = 2.593$. Although signals from interfering elements were monitored, the magnitude of the corrections was less than the internal analytical uncertainty and consequently insignificant. Typical beam intensity for ^{88}Sr was 5E-11 amperes and for ^{85}Rb was 2.5E-12 amperes.

Ar-Ar Isotopic Analyses

Infrared laser step-heating measurements for isotopic dating by the $^{40}Ar/^{39}Ar$ method were conducted at the Berkeley Geochronology Center, in Berkeley, CA, USA. Prior to analyses, two aliquots of NWA 4734 (3.42 and 4.18 mg, respectively) were irradiated for 100 h in a Cd-shielded (to minimize undesirable isotopic interference reactions) CLICIT facility of the TRIGA reactor at Oregon State University. Samples and the neutron fluence monitor PP-20 hornblende (the same as Hb3gr) were loaded into pits within aluminum disks. The J-value of 0.0264489 ± 0.00021 was calculated relative to an age of Hb3gr = 1072 ± 11 Ma (Turner 1971) and using the decay constants of Steiger and Jäger (1977). The correction factors for interfering isotopes correspond to the weighted mean of 10 yr of measurements of K–Fe and $CaSi_2$ glasses and CaF_2 fluorite in the TRIGA reactor: $(^{39}Ar/^{37}Ar)_{Ca} = (7.60 \pm 0.09) \times 10^{-4}$, $(^{36}Ar/^{37}Ar)_{Ca} = (2.70 \pm 0.02) \times 10^{-4}$, and $(^{40}Ar/^{39}Ar)_K = (7.30 \pm 0.90) \times 10^{-4}$. The two NWA 4734 aliquots were degassed separately using a defocused CO_2 laser. The gas was purified in a stainless steel extraction line using two C-50 getters and a cryogenic condensation trap. Argon isotopes were measured in static mode using a MAP 215–50 mass spectrometer with a Balzers electron multiplier, primarily using 10 cycles of peak-hopping. A detailed description of the mass spectrometer and extraction line is given by Renne et al. (1998). Blank measurements were generally obtained after every three sample runs. Ar isotopic data are corrected for blank, mass discrimination, and radioactive decay. Further details of

Table 1. Modal mineralogy of NWA 4734, NWA 032, and the LAP meteorites.

Sample	NWA 4734	NWA 4734	NWA 032	LAP Averages					
Reference	This study[a]	1	2	3	4	5	6	7	8
Pyroxene	58.1	58.0 ± 2.5	4.8[b]	48.9 ± 2.5	50.4 ± 3.8	54.6 ± 1.1	58.7 ± 1.0	56.9	56.2
Plag/Mask	25.0	30.6 ± 3.4	–	32.7 ± 1.3	38.9 ± 4.0	33.4 ± 1.2	32.1 ± 0.4	33.1	31.9
Olivine	6.5	3.8 ± 2.2	11.3[b]	3.0 ± 0.6	1.7 ± 0.6	1.6 ± 0.8	2.3 ± 0.8	1.2	1.5
Ilmenite	2.9	2.2 ± 1.1	–	3.8 ± 0.2	4.1 ± 0.8	3.4 ± 0.2	2.9 ± 0.3	3.3	3.3
Spinels	0.6	0.7 ± 0.2	0.3[b]	0.4 ± 0.05	0.8 ± 0.5	0.5 ± 0.1	0.5 ± 0.4	0.5	1.0
Silica	1.8	1.5 ± 0.7	–	2.0 ± 0.2	–	–	0.5 ± 0.1	2.3	–
Fayalite	3.0	–	–	3.6 ± 0.9	2.1 ± 0.8	1.7 ± 0.3	1.0 ± 0.6	1.5	–
Sulfide	0.3	0.1 ± 0.1	–	0.2 ± 0.01	0.9 ± 0.5	0.2 ± 0.02	–	0.2	0.1
Phosphate	0.4	–	–	–	1.1 ± 0.5	0.2 ± 0.03	–	0.3	–
K-spar/Si-K-Glass	1.5	0.3 ±	–	–	–	0.7 ± 0.1	–	–	–
Shock melt	na	2.3 ± 1.4	3.2	0.6 ± 1.1	–	1.7 ± 0.4	–	0.8	0.7
Groundmass phases	–	–	80.4[c]	–	–	–	–	–	–

[a]Void space subtracted and normalized to 100%. Trace baddeleyite, metal, tranquillityite, and zirconolite also present.
[b]Phenocrysts only.
[c]Groundmass consists of pyroxene, feldspar, ilmenite, and sulfide. na = Not present in section. Uncertainties are 1σ standard deviations of multiple modal analyses, where available.
References: (1) Wang et al. 2012; (2) Fagan et al. 2002; (3) Zeigler et al. 2005; (4) Righter et al. 2005; (5) Day et al. 2006; (6) Joy et al. 2006; (7) Anand et al. 2006; (8) Hill et al. 2009.

data reduction procedures are given in Burgess and Turner (1998), Renne et al. (1998), Fernandes et al. (2000, 2003), and Fernandes and Burgess (2005).

RESULTS

Petrographic descriptions of NWA 032/479 and LAP have been provided previously by numerous authors; however, only one study has focused on NWA 4734 (Wang et al. 2012), so in the following sections, we focus on providing geochemical, textural, and mineralogic descriptions of NWA 4734 with comparisons to LAP and NWA 032.

Textures and Mineral Chemistry

The modal mineralogy determined from a 24 mm^2 area (Fig. 1a) of NWA 4734 is given in Table 1, along with the modal mineralogy of LAP and NWA 032. NWA 4734 is a relatively coarse-grained basalt with a subophitic texture. BSE images showing typical textures in NWA 4734 are presented in Fig. 1, and BSE images comparing textures with those of NWA 032 and LAP are shown in Fig. 2. NWA 4734 is dominated by subhedral to anhedral pyroxene and plagioclase, which is mostly converted to maskelynite, with minor amounts of ilmenite and forsteritic olivine. It also contains trace amounts of chromite; chromian ülvospinel; ülvospinel; sulfides; Fe-metal; and a groundmass dominated by fayalite and a silica polymorph with accessory K-feldspar, fluorapatite, merrillite, and baddeleyite. Zirconolite and tranquillityite, although unobserved in this study, were reported by Connolly et al. (2008) and Wang et al. (2012). Melt veins of basaltic composition, probably the result of shock, are also present. Mineral phases, with the exception of maskelynite, are highly fractured (Fig. 1). A schematic comparison of the crystallization sequences of the three basalts is shown in Fig. 3.

Forsteritic olivine grains in NWA 4734 are typically anhedral and vary in size from tens of μm to approximately 1 mm in the longest direction. Occasionally, small, relatively unzoned, Mg-rich olivine grains are found as inclusions within pigeonite (e.g., Fig. 1b), and most olivine is at least partially surrounded by pyroxene with an uneven boundary. Similar textural relationships with pyroxene and the presence of small, Mg-rich, unzoned olivines (possibly relict cores) within pigeonite grains may be evidence of olivine resorption in LAP (Zeigler et al. 2005). Larger olivine grains are normally zoned and range in composition from $Fo_{64–34}$ (Fig. 4a). The olivine core composition gives an olivine-bulk rock K_D of 0.32, indicating no significant crystal accumulation. Representative analyses of olivine in NWA 4734 are shown in Table 2 and all analyses are in Table S2. Figure 5 shows a plot of SIMS analyses of Ni and Co in olivine from all three meteorites (Table S3), along with analyses of NWA 032 olivine from Borg et al. (2009). All three meteorites have overlapping Ni/Co and are distinct from the Apollo 12 low-Ti basalts and other lunar crustal lithologies (Shearer and Papike 2005; Longhi et al. 2010).

Chromite grains are often found in close association with, or included within, olivine grains. Chromite is usually intergrown with chromian ülvospinel. Ülvospinel

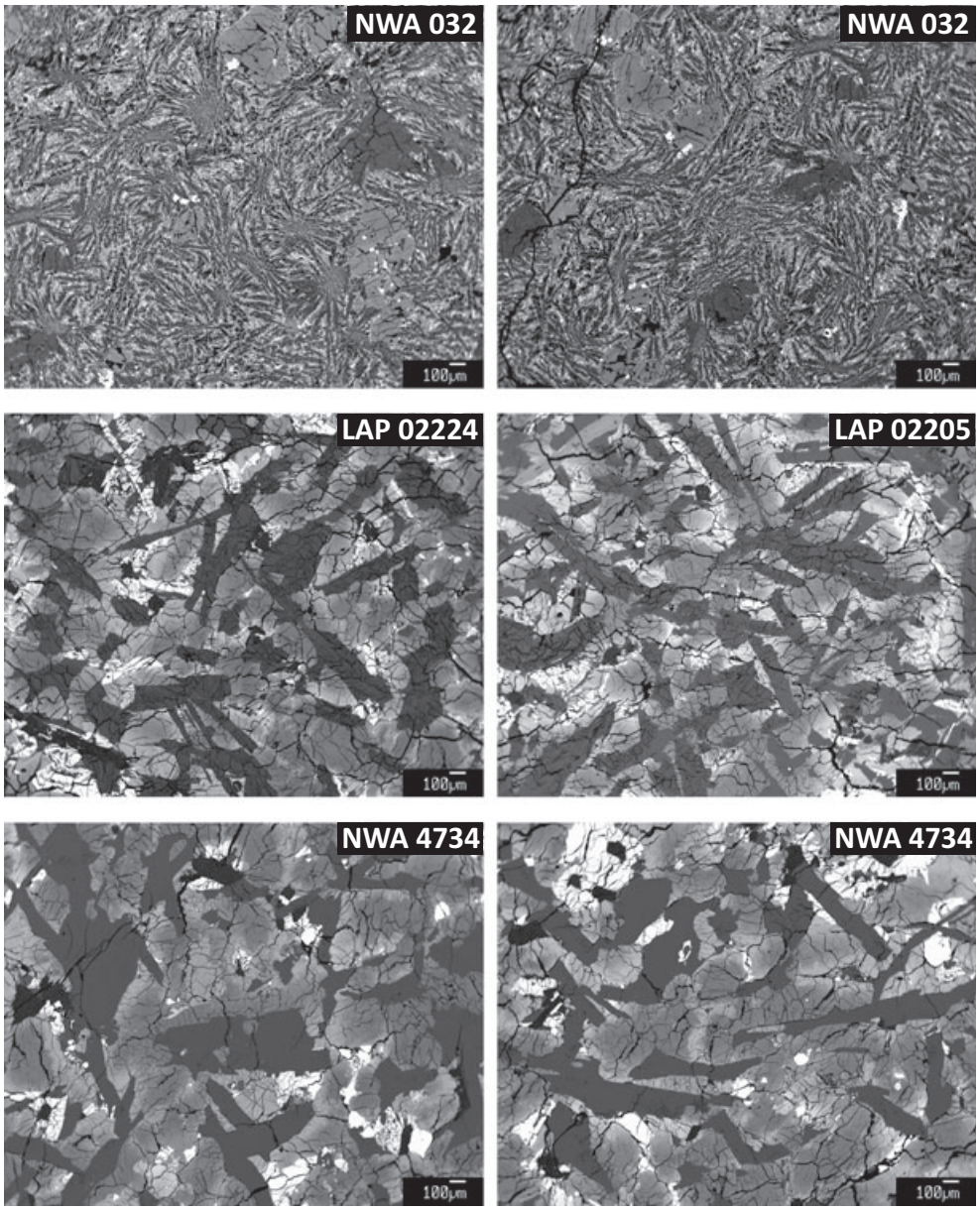


Fig. 2. BSE images of NWA 032, LAP, and NWA 4734 comparing textures. All images are at the same magnification.

grains are sometimes found included within pyroxene grains. Spinel compositions span nearly the full range between the endmembers (Fig. S2). Ilmenite grains usually form elongate laths sometimes hundreds of μm in length, but also occur as smaller grains along phase boundaries and in the groundmass. Compositions do not vary significantly from the endmember ilmenite composition. All EMP analyses of oxides in NWA 4734, NWA 032, and LAP are presented in Table S4.

Pyroxene is the most abundant phase in NWA 4734 (Table 1). Pyroxene grains occur as anhedral and/or irregularly shaped grains that often partially enclose feldspar. Compositions for all three meteorites are shown in Fig. 4. Pyroxenes in NWA 4734 range from pigeonite to augite, and then continuously increase in Fe through ferroaugite toward hedenbergite. A few compositions trend toward pyroxferroite. This seems rare compared with LAP pyroxenes in our data set (Fig. 4a); however, Zeigler et al. (2005) saw significant variability among subsamples of the LAP stones. Representative EMP analyses of pyroxenes in NWA 4734 are shown in Table 2 and all analyses for NWA 4734, NWA 032, and LAP are presented in Table S5. A plot of Ti/Al for pyroxenes in all three meteorites is shown in Fig. 6. Al and Ti abundances are correlated with Mg* in NWA 4734 and LAP and initially increase

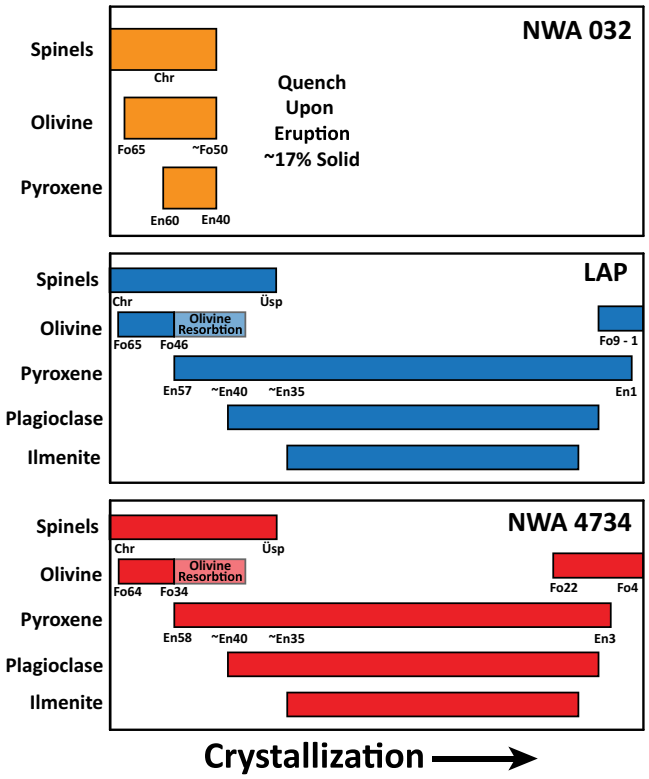


Fig. 3. A schematic representation of the approximate crystallization sequences for NWA 032, LAP, and NWA 4734. Approximate ranges in mineral compositions are shown along with the approximate pyroxene compositions at the times of plagioclase and ilmenite saturation, which are deduced from compositional constraints.

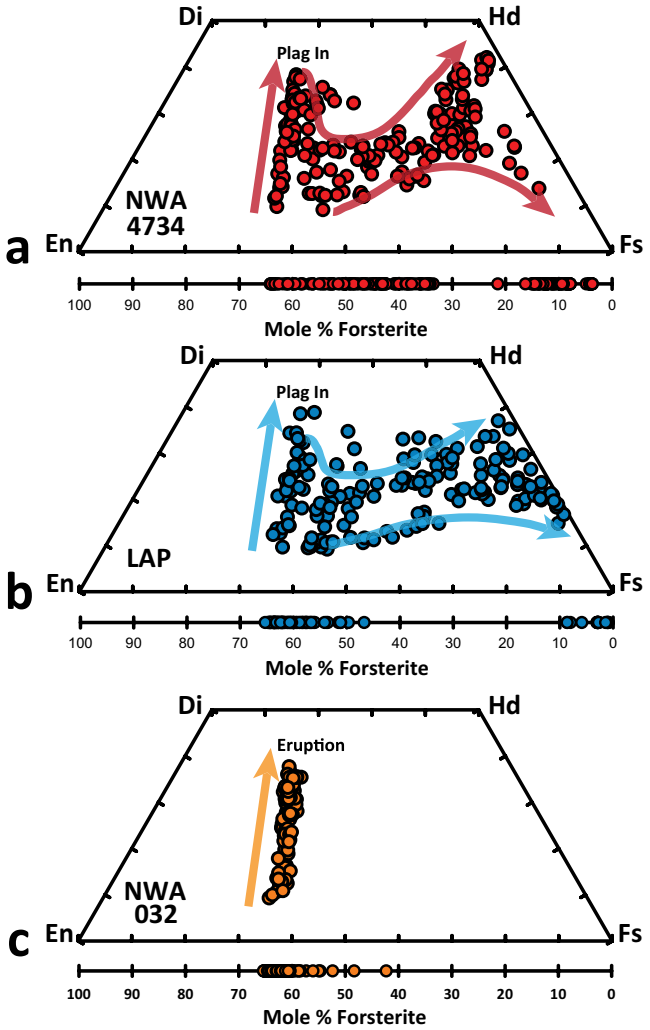


Fig. 4. Major element compositions of pyroxene and olivine for NWA 4734, NWA 032, and LAP. Crystallization trends in the pyroxene quadrilateral are schematic and are inferred from textures and compositional constraints. All data are from this study. In figures throughout this paper, NWA 032 data will appear in orange symbols, LAP in blue, and NWA 4734 in red.

with decreasing Mg* while maintaining a ratio of 1:4. This is followed by a change in Ti/Al between 1:2 and 3:4, at which point abundances begin to decrease. The change in Ti/Al is a reflection of the appearance of plagioclase on the liquid line of descent. This behavior has been described in other mare basalts by Bence and Papike (1972). An increase of the Ti/Al ratios above 1:2 has been attributed to incorporation of additional Ti^{3+} via the component $R^{2+}Ti^{3+}AlSiO_6$. Pyroxenes in LAP and NWA 4734 also show excellent correlation on a plot of Ti/Ca versus Mg* (Fig. 7), which can be used to determine the point of ilmenite saturation. This occurs at a pyroxene Mg* of approximately 37 for both basalts.

Qualitative WDS maps of Mg, Ti, and Cr in representative pyroxenes from all three meteorites are shown in Fig. 8 to illustrate zoning. Normal zoning patterns in pyroxene are observed in LAP and NWA 4734, with the pyroxenes having Mg-rich cores and Mg-poor rims. Ti concentrations first increase from pyroxene moving outward from the core, reflecting the overall incompatible behavior of Ti until ilmenite saturation, at which point Ti abundances decrease in LAP and NWA 4734. Cr concentrations decrease from core to rim, reflecting the crystallization of chromite and chromian ülvospinel, and the compatible behavior of Cr in pyroxene. These zoning patterns differ from the oscillatory zoning in major and minor elements observed in NWA 032 (Burger et al. 2009). Elardo and Shearer (2014) concluded that oscillatory zoning patterns in NWA 032 are a result of varying liquid compositions experienced by the grains as they were convected through a differentially cooling magma chamber.

Plagioclase grains in NWA 4734 typically form elongate laths that are partially surrounded by

Table 2. Representative EMP analyses of NWA 4734 olivine and pyroxene.

Wt%	Ol.	Ol.	Ol.	Ol.	Ol.	Ol.	Ol.
SiO_2	36.4	35.4	33.8	32.7	31.8	30.1	30.1
TiO_2	0.03	0.02	0.05	0.06	0.25	0.13	0.24
Al_2O_3	0.06	0.27	0.02	0.47	0.03	nd	0.02
Cr_2O_3	0.08	0.08	0.09	0.05	0.05	nd	nd
FeO	32.1	33.9	41.7	46.2	51.7	62.9	66.4
MnO	0.30	0.34	0.43	0.44	0.51	0.67	0.78
MgO	31.4	29.4	23.8	19.1	14.7	5.18	1.63
CaO	0.23	0.36	0.36	0.39	0.37	0.59	0.70
Na_2O	nd	nd	nd	nd	nd	nd	nd
P_2O_5	nd	0.03	nd	nd	0.03	0.03	0.11
Total	100.64	99.75	100.22	99.42	99.51	99.60	100.00
Stoichiometry based on 4 oxygens							
Si	0.989	0.981	0.974	0.974	0.978	0.986	1.003
Ti	0.001	0.000	0.001	0.001	0.006	0.003	0.006
Al	0.002	0.009	0.001	0.016	0.001	–	0.001
Cr	0.002	0.002	0.002	0.001	0.001	–	–
Fe^{2+}	0.730	0.785	1.003	1.151	1.329	1.726	1.846
Mn	0.007	0.008	0.010	0.011	0.013	0.019	0.022
Mg	1.270	1.215	1.022	0.849	0.672	0.253	0.081
Ca	0.007	0.011	0.011	0.012	0.012	0.021	0.025
P	–	0.001	–	–	0.001	0.001	0.003
Σ Cations	3.008	3.012	3.024	3.016	3.014	3.009	2.986
Mg*	63.5	60.7	50.5	42.5	33.6	12.8	4.2

Wt%	Aug.	Aug.	Pig.	Pig.	Pig.	Fe. Aug.	Hd.	Pyxfer.
SiO_2	49.7	50.1	49.9	48.7	47.4	46.9	46.4	46.9
TiO_2	1.16	1.06	0.98	1.01	0.92	1.07	1.23	0.94
Al_2O_3	2.77	2.53	2.51	1.49	1.03	1.23	1.51	0.89
Cr_2O_3	0.92	0.82	0.81	0.36	0.14	0.15	0.12	0.02
FeO	14.6	16.5	17.3	27.1	33.5	33.3	30.2	38.8
MnO	0.29	0.32	0.32	0.42	0.46	0.44	0.39	0.50
MgO	14.7	15.7	15.9	11.4	5.68	4.42	2.96	2.16
CaO	15.0	12.5	11.7	9.01	10.4	11.9	16.1	9.87
Na_2O	0.04	0.03	0.04	nd	nd	0.02	0.02	0.02
P_2O_5	nd	nd	nd	nd	nd	nd	nd	nd
Total	99.13	99.52	99.56	99.51	99.58	99.52	99.01	100.15
Stoichiometry based on 6 oxygens								
Si	1.891	1.903	1.895	1.926	1.946	1.935	1.924	1.962
Al^{iv}	0.109	0.097	0.105	0.070	0.050	0.060	0.074	0.038
Σ T-site	2.000	2.000	2.000	1.995	1.996	1.995	1.998	2.000
Al^{vi}	0.015	0.016	0.007	0.000	0.000	0.000	0.000	0.006
Ti	0.033	0.030	0.028	0.030	0.029	0.033	0.038	0.030
Cr	0.028	0.025	0.024	0.011	0.004	0.005	0.004	0.001
Mg	0.836	0.886	0.901	0.672	0.347	0.272	0.183	0.135
Fe^{2+}	0.461	0.524	0.529	0.886	1.149	1.150	1.046	1.356
Mn	0.009	0.010	0.010	0.014	0.016	0.015	0.014	0.018
Ca	0.612	0.507	0.476	0.382	0.457	0.527	0.716	0.442
Na	0.003	0.002	0.003	–	–	0.002	0.002	0.001
Σ Cations	3.998	3.999	3.979	3.991	3.999	3.999	4.000	3.987
Mg*	64.4	62.8	63.0	43.1	23.2	19.1	14.9	9.0
En	43.8	46.2	47.2	34.6	17.8	14.0	9.4	7.0
Fs	24.2	27.3	27.8	45.7	58.8	59.0	53.8	70.2
Wo	32.1	26.4	25.0	19.7	23.4	27.0	36.8	22.9

Ol. = olivine, Aug. = augite, Pig. = pigeonite, Fe. Aug = ferroaugite, Hd. = hedenbergite, Pyxfer. = approaching pyroxferroite, nd = not detected, Mg* = molar Mg/(Mg+Fe)*100.

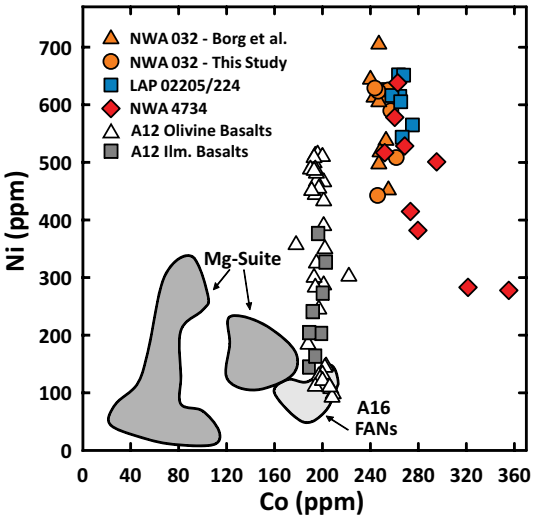


Fig. 5. A plot of the Ni and Co abundances in lunar olivine measured via SIMS. Data for NWA 4734, LAP, and NWA 032 are from this study. Our NWA 032 data are consistent with those of Borg et al. (2009). Apollo 12 mare basalt data from Papike et al. (1999) and Karner et al. (2003). Fields for the Mg-suite and FANs are from Shearer and Papike (2005).

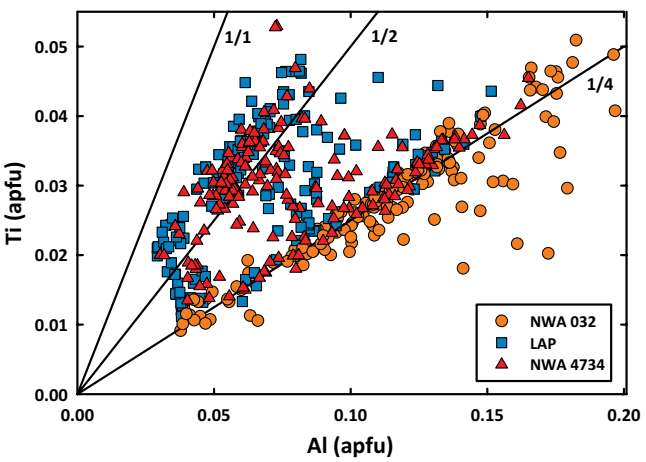


Fig. 6. Pyroxene Ti versus Al in atoms per formula unit (apfu) for NWA 4734, LAP, and NWA 032. Lines representing ratios of 1:4, 1:2, and 1:1 are shown to identify the dominant coupled substitutions (see text).

pyroxene. Most of the plagioclase has been converted to maskelynite (smooth dark gray phase in Figs. 1 and 2). Both plagioclase and maskelynite retain normal magmatic zoning with compositions ranging from $An_{90–80}$ (Fig. S3). All EMP analyses of plagioclase in NWA 4734 and LAP are presented in Table S6.

The groundmass of NWA 4734 is dominated by fayalite and a silica polymorph. Many fayalite grains in NWA 4734 are large and can be up to 500–600 μm in the longest direction with occasional silica inclusions (Fig. 1d). Fayalite compositions are shown in Fig. 4,

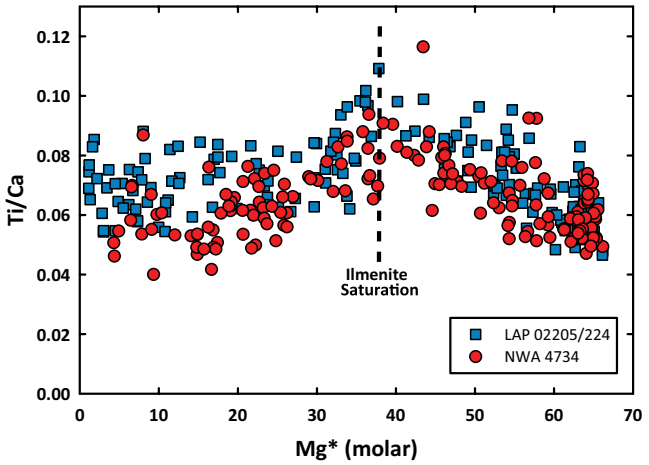


Fig. 7. Pyroxene Ti/Ca versus Mg* in NWA 4734 and LAP. A drop in Ti/Ca at Mg* approximately 37 is indicative of ilmenite saturation in the melt and occurs at the same point for both basalts.

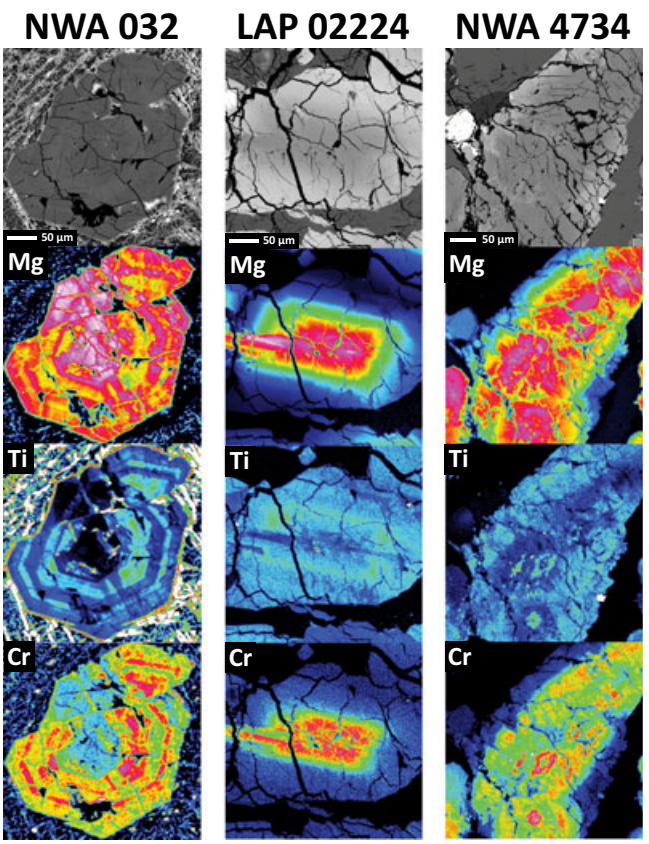


Fig. 8. BSE images and qualitative WDS maps of Mg, Ti, and Cr in pyroxene phenocrysts from NWA 032, LAP 02224, and NWA 4734. Pyroxenes in NWA 4734 and LAP show similar, normal magmatic zoning patterns, whereas pyroxenes in NWA 032 show oscillatory patterns. Warm colors are higher concentrations and cool colors are lower concentrations. Image and maps for NWA 032 from Elardo and Shearer (2014).

Table 3. Representative EMP analyses of NWA 4734 phosphates.

Wt%	Apatite	Apatite	Apatite	Apatite	Merr.	Merr.
P_2O_5	38.5	37.8	39.6	39.2	40.9	40.3
SiO_2	2.02	1.63	1.07	1.49	0.50	0.60
Ce_2O_3	1.00	0.58	0.39	0.31	2.74	2.93
Y_2O_3	0.66	0.90	0.46	0.56	2.75	2.95
FeO	1.48	1.47	2.33	1.05	6.71	6.88
MnO	0.06	0.04	0.04	0.01	nd	0.05
MgO	0.01	nd	0.03	0.02	0.27	0.27
CaO	52.2	51.7	52.1	53.2	39.0	38.7
Na_2O	0.02	nd	nd	nd	0.02	nd
F	2.59	2.81	2.81	2.64	nd	nd
Cl	0.37	0.29	0.12	0.27	0.03	0.05
S	0.03	0.03	0.08	0.02	nd	0.02
F + Cl = −O	1.19	1.26	1.24	1.19	0.01	0.02
Total	97.76	95.99	97.77	97.58	92.91	92.69
Stoichiometry based on 13 (apatite) and 56 (merrillite) anions						
Cations						
P	2.83	2.84	2.90	2.87	13.95	13.83
Si	0.18	0.14	0.09	0.13	0.20	0.24
Ce	0.03	0.02	0.01	0.01	0.40	0.44
Y	0.03	0.04	0.02	0.03	0.59	0.64
Fe	0.11	0.11	0.17	0.08	2.26	2.33
Mg	0.00	0.00	0.00	0.00	0.16	0.16
Ca	4.86	4.91	4.83	4.93	16.81	16.82
Na	0.00	0.00	0.00	0.00	0.01	0.00
Σ Cations	8.04	8.06	8.03	8.04	34.39	34.46
Anions						
F	0.71	0.79	0.77	0.72	0.00	0.00
Cl	0.05	0.04	0.02	0.04	0.02	0.04
S	0.01	0.00	0.01	0.00	0.00	0.02
Σ Anions	0.77	0.84	0.80	0.77	–	–
X-Def. (OH)	0.23	0.16	0.20	0.23	–	–

nd = not detected, Merr. = merrillite, X-Def. (OH) = 1 − (F+Cl+S).

and representative EMP analyses are in Table 2. Apatite and merrillite both occur in the late-stage crystallized melt pockets, with apatite being the more abundant phosphate. Representative EMP analyses of apatite and merrillite are shown in Table 3 and all analyses are presented in Table S7. Merrillite is rich in REEs. Apatite compositions from NWA 4734 are shown alongside analyses from LAP (McCubbin et al. 2011) in the F-Cl-OH ternary in Fig. 9. Apatite in NWA 4734 (and LAP) is fluorapatite with Cl occupying only 2–5% of the X-site (0.12–0.37 wt% Cl). However, structural OH^- (inferred from an X-site anion deficiency, where 1 − [F + Cl + S] = OH) occupies up to 24% of the X-site. Apatite grains in LAP and NWA 4734 are similar in composition to other mare basalts (McCubbin et al. 2011), but dissimilar to KREEP-rich highland lithologies (Fig. 9). Other observed phases in the groundmass include K-feldspar, sulfides, and baddeleyite.

Bulk-Rock Composition

The bulk-rock major, minor, and trace element composition of NWA 4734 is given in Table 4 (standard reference data are in Table S1), alongside the bulk-rock composition of the LAP basalts, NWA 032, and examples of low-Ti basalts from Apollo 12 and 15. NWA 4734 is an evolved mare basalt, and is classified as a low-Ti, low-Al, low-K mare basalt using the classification scheme developed by Neal and Taylor (1992). Its low MgO, moderate Al_2O_3 and CaO, and relatively low Mg* make it most similar to the Apollo 12 and Apollo 15 pigeonite basalts (Figs. 10a–c). The Apollo 12 and most Apollo 15 olivine basalts have a higher Mg* and a higher modal abundance of olivine (Papike et al. 1998). NWA 4734 also has lower TiO_2 (Fig. 10b) content than the Apollo 12 ilmenite basalts and slightly higher K_2O (Fig. 10d) than the Apollo 12 and Apollo 15 low-Ti basalt groups.

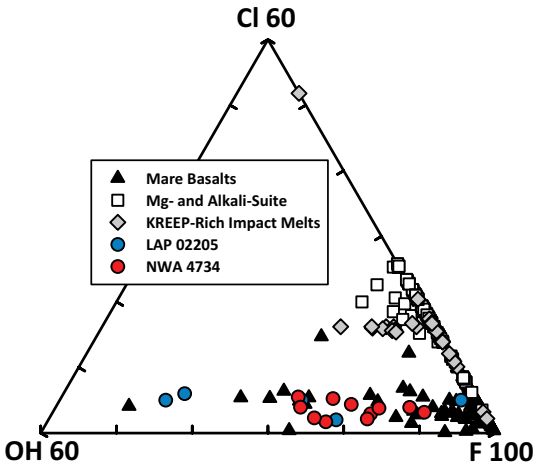


Fig. 9. Ternary F-Cl-OH compositions of lunar apatite, which shows the disparity between KREEP-poor/free lithologies (Cl-poor, OH-rich) and KREEP-rich lithologies (Cl-rich, OH-poor). NWA 4734 data are from this study. Data for LAP, other mare basalts, and KREEP-rich lithologies (Mg- and Alkali-suites, and impact melts) are from McCubbin et al. (2011).

Incompatible trace element concentrations (e.g., Zr, Hf, Nb, Y, Rb, Th, REEs) in NWA 4734, NWA 03 2, and LAP are higher than in Apollo 12 and Apollo 15 low-Ti basalts as well as low-Ti basaltic meteorites of similar Mg* (Figs. 11a–d). The differences between the three meteorites in Ba and Sr (Table 4) can be attributed to variations in the extent of desert weathering experienced by each meteorite. Compatible trace element concentrations (e.g., Ni, Co, Cr, V, Sc) usually fall well within the fields defined by the Apollo 12 and Apollo 15 basalts (Fig. 11e). Ni and Co in NWA 032 are slightly elevated (Ni/Co = 1.2), which is probably due to some accumulated olivine and chromite (see the Discussion section).

The chondrite-normalized REE pattern of NWA 4734 shows that it has a high LREE/HREE, with a $(La/Sm)_N$ of 1.09 and a $(La/Yb)_N$ of 1.29 (Figs. 11f and 12). NWA 4734 is enriched in REEs compared with the Apollo low-Ti basalts, with the exception of HREEs in the Apollo 12 ilmenite basalts. It also has a deeper

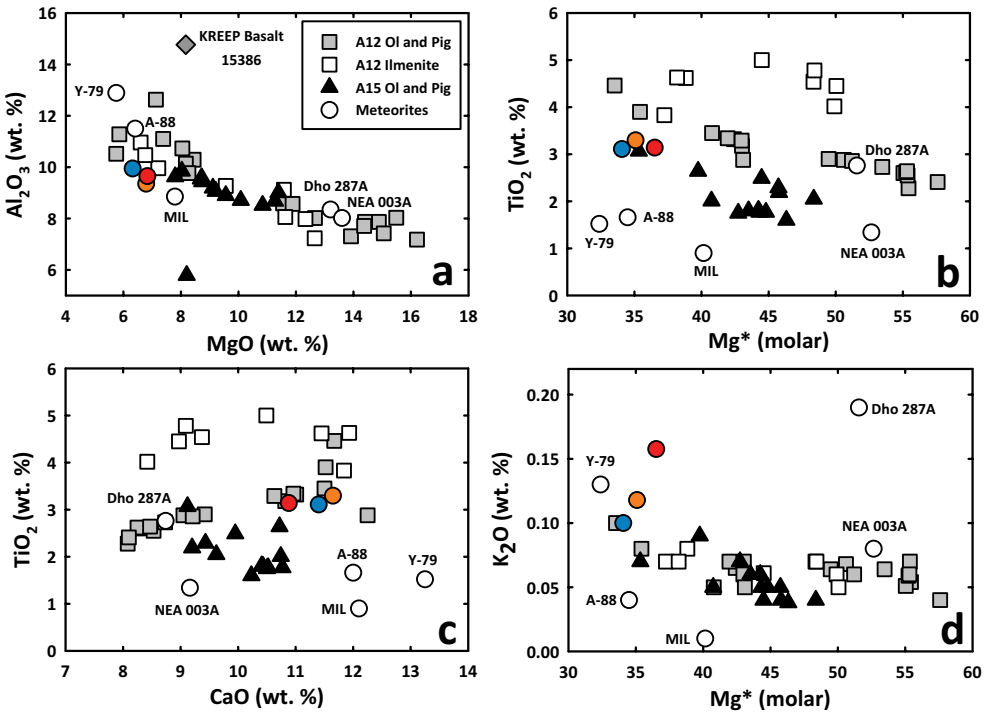


Fig. 10. Four plots showing the bulk major element composition of NWA 4734 (red), NWA 032 (orange), and LAP (blue), in addition to other unbrecciated basaltic lunar meteorites and major low-Ti mare basalt groups from Apollo 12 and 15. Mg* = molar (Mg/(Mg+Fe))*100. Data for NWA 4734 are from this study. Other lunar meteorite data from Fagan et al. (2002), Zeigler et al. (2005), Day et al. (2006), Anand et al. (2003), Koeberl et al. (1993), Yanai and Kojima (1991), Joy et al. (2008), Borg et al. (2009), and Haloda et al. (2009). Apollo 12 and 15 data from numerous sources and sample numbers are available upon request (Bouchet et al. 1971; Brunfelt et al. 1971, 1972; Compston et al. 1971, 1972; Cuttitta et al. 1971, 1973; Engel et al. 1971; Haskin et al. 1971; Hubbard and Gast 1971; Kushiro and Haramura 1971; Maxwell and Wiik 1971; Taylor et al. 1971; Wänke et al. 1971, 1975, 1976; Willis et al. 1971, 1972; Mason et al. 1972; O'Kelley et al. 1972; Chappell and Green 1973; Fruchter et al. 1973; Ganapathy et al. 1973; Helmke et al. 1973; Duncan et al. 1975; Nyquist et al. 1977; Rhodes et al. 1977; Warren et al. 1986; Neal et al. 1994a; Papike et al. 1998; Neal 2001; Ryder and Schuraytz 2001).

Table 4. Bulk compositions of NWA 4734 and selected low-Ti mare basalts.

Sample	NWA 4734	±	LAP	NWA 032	032 Calc[b]	12009	12031	12022	15545	15058
References	This Study		1, 2, 3	2, 4, 5	1	6, 7	6, 8	6, 9	6, 10	11–14
Classification						Ol. Bas.	Pig. Bas.	Ilm. Bas.	Ol. Bas.	Pig. Bas.
SiO_2	47.1[a]		45.3	44.7	45.2	45.03	47.0	42.3	44.9	48.5
TiO_2	3.14	0.01	3.11	3.00	3.21	2.90	2.88	4.54	2.49	1.60
Al_2O_3	9.65	0.03	9.79	9.32	10.0	8.59	12.6	9.12	8.71	8.90
Cr_2O_3	0.30	0.002	0.31	0.40	0.31	0.55	0.35	0.60	0.54	0.66
FeO	21.2	0.02	22.2	22.2	22.2	21.0	16.8	22.1	22.4	19.8
MnO	0.28	0.001	0.29	0.28	0.29	0.28	0.26	0.26	0.31	0.27
MgO	6.83	0.02	6.63	7.97	6.63	11.6	7.13	11.6	10.1	9.56
CaO	10.9	0.01	11.1	10.6	11.1	9.42	12.3	9.37	9.95	10.2
Na_2O	0.36	0.002	0.38	0.35	0.38	0.23	0.33	0.29	0.45	0.28
K_2O	0.16	0.001	0.07	0.09	–	0.06	0.05	0.07	0.04	0.04
P_2O_5	–		0.10	0.09	0.10	0.07	0.05	0.02	0.07	0.05
Total	99.86		99.28	99.0	99.21	99.71	99.68	100.24	96.96	99.81
Mg*	36.5		34.7	39.0	34.7	49.5	43.1	48.3	44.5	46.3
Trace element concentrations and uncertainties in ppm										
Li	11.53	0.03	13.5	–		7.21	3.85	9.27	8.3	–
Be	0.99	0.09	1.14	–		0.62	0.81	0.87	0.54	–
Sc	50.0	2.3	56.8	56		45.7	49.5	59.6	43.9	46
V	113.9	11.6	108.0	–		186	128	156	308	–
Cr	2029	193	2159.2	–		4229	1934	3004	6444	4516
Co	34.7	2.2	37.03	42		–	28	–	61.5	42
Ni	28.3	0.9	25.20	50		61	4.21	29.1	70.4	31
Cu	12.0	0.1	18.77	–		12.8	14	15.7	14.3	–
Zn	36.4	3.8	28.6	–		6.64	16.9	11.3	19.7	–
Ga	3.59	0.11	4.02	–		2.82	3.43	3.64	3.57	–
Rb	2.12	0.004	1.73	–		1.08	1.09	0.78	0.87	2
Sr	162.5	3.4	117.5	142		99.6	126.9	147.5	106.3	99.2
Y	66.2	0.6	61.73	52.8		34.2	35.9	50.7	29.3	21.2
Zr	205.6	2.4	181.8	175		112.3	92.5	121.7	89.2	70.9
Nb	14.8	0.2	12.53	–		6.54	6.50	5.98	6.31	4.9
Cs	0.04	0.01	0.03	–		0.04	0.05	0.03	0.02	–
Ba	152.3	2.2	128.3	242		63.4	58.5	56.8	49.2	62
La	12.32	0.004	11.01	11.29		5.86	5.22	5.59	4.60	5.58
Ce	32.8	0.2	28.48	30.58		16.3	15.6	16.9	13.4	14.5
Pr	4.55	0.09	4.39	4.22		2.58	2.40	2.93	2.02	–
Nd	22.96	0.02	20.70	20.68		12.4	11.4	15.3	9.30	10.9
Sm	7.24	0.01	6.51	6.68		4.62	3.93	5.63	3.41	3.9
Eu	1.22	0.02	1.05	1.14		0.89	1.04	1.30	0.83	0.91
Gd	10.2	1.0	8.53	8.55		6.33	5.40	8.74	4.44	5
Tb	1.71	0.02	1.57	1.62		1.00	0.94	1.48	0.73	0.87
Dy	11.66	0.01	10.11	10.56		6.96	6.35	10.2	4.57	5.59
Ho	2.46	0.02	2.17	2.26		1.4	1.33	2.09	0.91	1.1
Er	6.7	0.3	5.83	6.58		4.11	3.88	6.13	2.46	3.2
Tm	0.99	0.01	0.91	0.90		0.57	0.53	0.84	0.31	–
Yb	6.5	0.1	5.70	5.81		3.86	3.48	5.51	2.12	2.54
Lu	0.91	0.0004	0.88	0.830		0.5	0.48	0.77	0.27	0.39
Hf	5.15	0.06	4.77	5.00		3.26	2.87	4.25	2.15	2.6
Ta	0.61	0.01	0.64	0.62		0.4	0.39	0.39	0.36	0.46
W	0.51	0.01	0.75	–		0.17	0.11	0.16	0.01	–
Pb	0.54	0.05	0.78	–		0.31	0.44	0.29	0.22	–
Th	2.00	0.002	1.95	1.9		0.9	0.82	0.63	0.41	0.52
U	0.48	0.01	0.48	0.45		0.24	0.22	0.19	0.12	0.13

[a]Determined by difference.

[b]Calculated bulk composition removing accumulated phases, see (1). References: (1) Zeigler et al. 2005; (2) Day et al. 2006; (3) Joy et al. 2006; (4) Fagan et al. 2002; (5) Borg et al. 2009; (6) Neal 2001; (7) Compston et al. 1971; (8) Rhodes et al. 1977; (9) Kushiro and Haramura 1971; (10) Chappell and Green 1973; (11) Helmke et al. 1973; (12) Willis et al. 1972; (13) O'Kelley et al. 1972; (14) Fruchter et al. 1973.

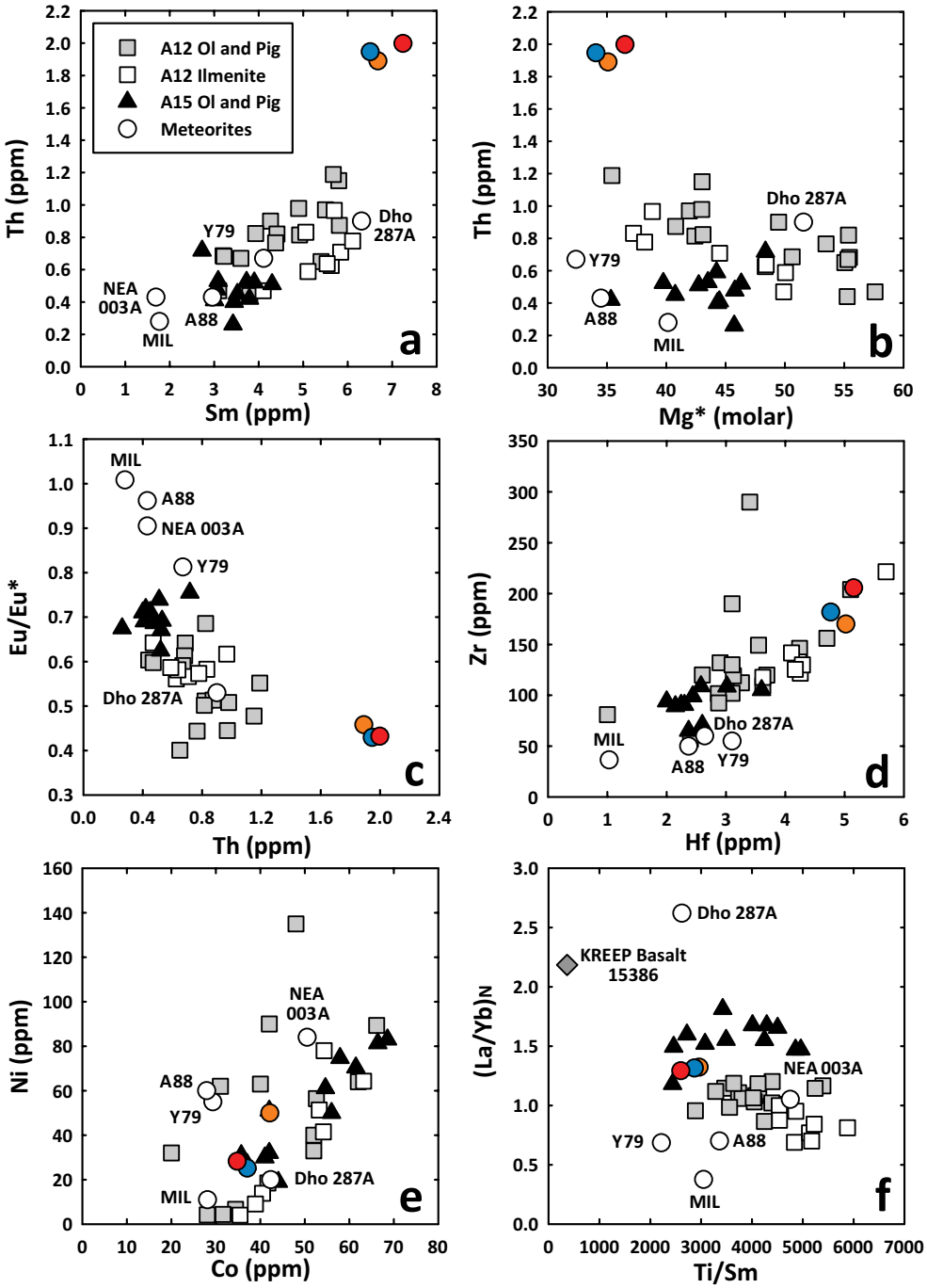


Fig. 11. Minor and trace element compositions of basaltic lunar meteorites and low-Ti basalts from Apollo 12 and 15. Data sources in Fig. 10 caption. NWA 032 in orange, LAP in blue, NWA 4734 in red.

negative Eu anomaly than most Apollo 12 and Apollo 15 low-Ti basalts, with Eu/Eu* (=Eu/[0.5*(Sm + Gd)]$_N$) of 0.43 (Fig. 11c) that is essentially identical to that of NWA 032 and LAP (0.46 and 0.43, respectively). NWA 032 and LAP have identical $(La/Sm)_N$ and $(La/Yb)_N$ of 1.08 and 1.32, respectively, which are in turn nearly identical to NWA 4734 (1.09 and 1.29, respectively). Despite similarities to each other, NWA 4734, NWA 032, and LAP have distinct REE patterns compared with other mare basaltic meteorites (Fig. 12b).

Sm-Nd and Rb-Sr Ages and Isotopic Compositions

Sm-Nd Isochron and Initial ε_{Nd}

A Sm-Nd isochron age of 3024 ± 27 Ma for NWA 4734 (Fig. 13) was determined from two 2 N HCl

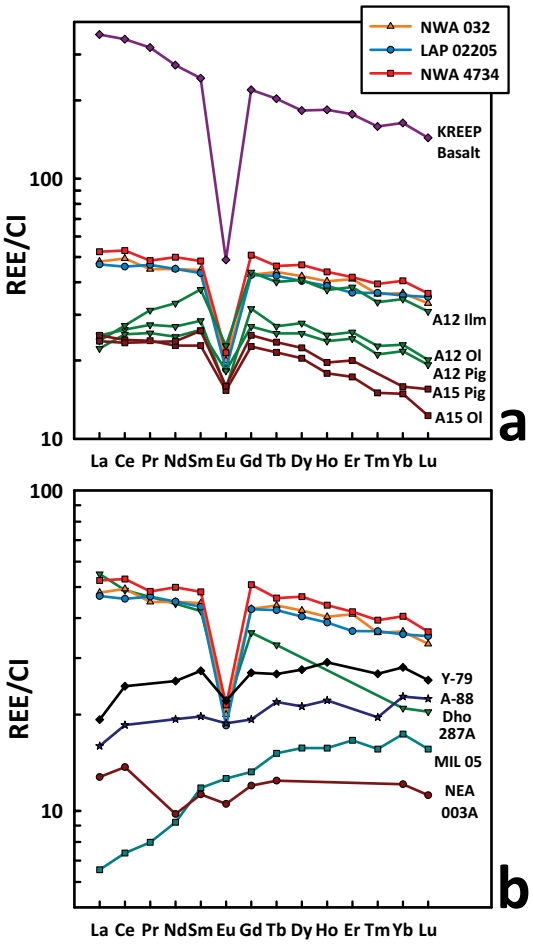


Fig. 12. Chondrite-normalized rare earth element plots for NWA 4734 (red), NWA 032 (orange), and LAP (blue) compared with low-Ti basalts from Apollo 12 and 15, in addition to KREEP basalt 15386 (Rhodes and Hubbard 1973; Neal and Kramer 2003) (a), and to other basaltic lunar meteorites (b). Note the different vertical scale in (b). Data sources in Fig. 10 caption. CI chondrite composition used is that of Lodders and Fegley (1998; and references within).

leached pyroxene fractions (Mg-Px and Fe-Px), the 2 N HCl leached plagioclase fraction, the 4 N HCl leached whole-rock residue (Wr-1 R), and the 1 N HCl leached whole-rock residue (Wr-2 R). The 4 N HCl whole-rock leachate (Wr-1 4L) lies off of the isochron, reflecting the presence of desert weathering products. The isochron yields an initial $\varepsilon_{Nd} = +0.88 \pm 0.20$ ($\varepsilon_{Nd} = [^{143}Nd/^{144}Nd_{sample}/^{143}Nd/^{144}Nd_{CHUR\ @\ 3024\ Ma} - 1] \times 10^4$). Samarium IC measurements were also made on NWA 4734 to correct for neutron capture effects (Russ et al. 1971; Nyquist et al. 1995). These measurements resulted in an ε_{149Sm} of −46.3 and an ε_{150Sm} of 85.4. The Sm-Nd isotopic compositions of all fractions are shown in Table 5.

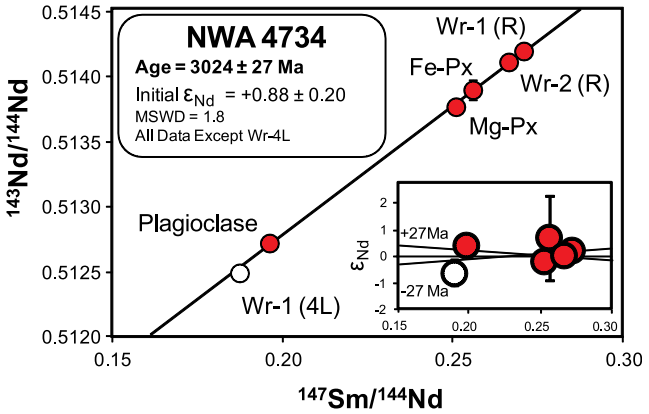


Fig. 13. Sm-Nd isochron plot of NWA 4734 mineral fractions. An age of 3024 ± 27 Ma is defined by the residue mineral and whole-rock fractions (red symbols). Secondary alteration has not affected the Sm-Nd isotopic systematics of these fractions, although it is apparent in the 2N (not shown) and 4N HCL leachates. Inset represents deviation of individual mineral fractions from the isochron in epsilon units ($[^{143}Nd/^{144}Nd]^{sample}/[^{143}Nd/^{144}Nd]^{isochron} - 1) \times 10^4$. The initial ε_{Nd} is calculated using the algorithm of Fletcher and Rosman (1982), and the isochron was calculated using the IsoPlot program of Ludwig (2001).

Rb-Sr Isochron and Initial $^{87}Sr/^{86}Sr$

The Rb-Sr systematics of NWA 4734 (Table 6) exhibit the effects of terrestrial contamination. However, a two-point tie line between the plagioclase fraction and the 4 N HCl leached whole-rock residue Wr-1 (R) results in an age of 3083 ± 42 Ma (Fig. 14). The initial $^{87}Sr/^{86}Sr$ ratio calculated from this tie line is 0.699867 ± 13 (uncertainty refers to the last digits). The 2 N HCl leached pyroxene fractions and the 4 N HCl whole-rock leachate lie above this tie line, probably indicating desert weathering contamination from carbonates rich in Sr (e.g., Borg et al. 2009). Although the above age is determined from a two-point tie line and therefore does not provide robust age information by itself, the plagioclase and whole-rock residue are the fractions most likely to preserve chronologic information due to the high concentrations of Sr in plagioclase and the extensive leaching procedure (2N followed by 4N HCl) undergone by the whole-rock fraction. Conversely, the two pyroxene fractions have low concentrations of Sr, making them more susceptible to desert alteration and the whole-rock leachate concentrates contaminants removed from the WR-1 residue. Our two-point tie line yields an age and initial $^{87}Sr/^{86}Sr$ ratio similar to those of Rankenburg et al. (2007) and Nyquist et al. (2005) for LAP, and concordant with the Sm-Nd age discussed above. Plots of the initial Sr and Nd isotopic compositions of all three meteorites are shown in Fig. 15.

Table 5. NWA 4734 Sm-Nd isotopic data

Fraction	Wt (mg)	Sm (ppm)[a]	Sm (ng)	Nd (ppm)[a]	Nd (ng)	$\frac{^{147}Sm}{^{144}Nd}$[a,d]	$\frac{^{143}Nd}{^{144}Nd}$[b]
Wr-1 (R)	26.98	2.227	60	4.985	134	0.27009 ± 27	0.514153 ± 7
Wr-1 (2L)			49		118	0.24891 ± 25	0.514180 ± 4
Wr-1 (4L)			6		18	0.18820 ± 19	0.512452 ± 22
Wr-2 (R)	33.28	2.119	70	4.818	160	0.26591 ± 27	0.514066 ± 4
Plagioclase	38.01	0.702	27	2.160	82	0.19641 ± 20	0.512679 ± 10
Fe-Pyroxene	52.97	4.048	214	9.679	513	0.25283 ± 36	0.513870 ± 80
Mg-Pyroxene	51.98	2.221	115	5.372	279	0.24990 ± 25	0.513738 ± 7
JNdi Nd Std (N = 8)					~100		0.512001 ± 10[c]

(2L) = 25 °C 2N HCl leachate, (4L) = 65 °C 4N HCl leachate, (R) = residue, (WR) = whole rock. All samples and standards run as Nd^+.

[a]Error limits apply to last digits and include a minimum uncertainty of 0.5% plus 50% of the blank correction for Sm and Nd added quadratically.

[b]Normalized to $^{146}Nd/^{144}Nd = 0.7219$. Uncertainties refer to last digits and are $2\sigma_m$ (2 × standard error of measured isotopic ratios).

[c]Uncertainties refer to last digits and are $2\sigma_p$ (2 × standard deviation of population of mass spectrometry runs on isotopic standard). Isochron is calculated using either $2\sigma_p$ (from standard runs) or $2\sigma_m$ (from measured isotopic ratios), whichever is larger.

[d]$^{147}Sm/^{144}Nd$ corrected for neutron capture based on measured Sm isotopic composition of $\varepsilon_{Sm}{}^{149} = -46.3 \pm 0.2$ measured on Wr-2 (R) fraction.

Table 6. NWA 4734 Rb-Sr isotopic data.

Fraction	Wt (mg)	Rb (ppm)	Rb (ng)	Sr (ppm)	Sr (ng)	$\frac{^{87}Rb}{^{86}Sr}$[a]	$\frac{^{87}Sr}{^{86}Sr}$[b]
Wr-1 (R)	26.98	1.427	38	82.36	2222	0.05013 ± 50	0.702082 ± 8
Wr-1 (4L)			3.0		822	0.01062 ± 11	0.700766 ± 10
Plagioclase	38.01	0.882	34	335.3	12744	0.00761 ± 8	0.700204 ± 6
Fe-Pyroxene	52.97	2.529	134	42.14	2232	0.1737 ± 17	0.708304 ± 8
Mg-Pyroxene	51.98	1.383	72	103.42	5375	0.03869 ± 39	0.702010 ± 8
NBS-987 (N = 12)					~100		0.710248 ± 10[c]

Wr = whole rock, (R) = residue from leaching procedure, (4L) = 65 °C 4N HCl leachate, (2L) = 25 °C 2N HCl leachate. The long-term $^{85}Rb/^{87}Rb$ measured on 30 runs of NBS-984 Rb standard = 2.603 ± 17 ($2\sigma_p$) and was used to corrected for instrument mass fractionation.

[a]Error limits apply to last digits and include a minimum uncertainty of 1% plus 50% of the blank correction for Rb and Sr added quadratically.

[b]Normalized to $^{86}Sr/^{88}Sr = 0.1194$. Uncertainties refer to last digits and are $2\sigma_m$ (2 × standard error of measured isotopic ratios).

[c]Uncertainties refer to last digits and are $2\sigma_p$ (2 × standard deviation of population of mass spectrometry runs on isotopic standard). Isochron is calculated using either $2\sigma_p$ (from standard runs) or $2\sigma_m$ (from measured isotopic ratios), whichever is larger.

Ar-Ar Step-Heating Results

^{40}Ar-^{39}Ar Age

An ^{40}Ar–^{39}Ar age of 2.717 ± 0.010 Ga is calculated based on the total $^{40}Ar/^{39}Ar$ (average from the indistinguishable ages calculated for the two aliquots). The ^{40}Ar-^{39}Ar step-heating data for the two bulk fragments of NWA 4734 are reported in Table S8 and age-spectrum is shown in Fig. S4. All uncertainties reported in Table S8 are at the 1σ level. A total of 26 and 25 heating steps were obtained from aliquots 1 and 2 of NWA 4734, respectively. The spectra for the aliquots are affected by ^{39}Ar-recoil effects: a continuous decrease of apparent age from the low- to high-temperature heating steps and a negative y-intercept. In the Ca/K release spectrum, there is a progressive increase from the low- to the high-temperature steps, which is suggestive of a gradual predominance in the release from a phase with relatively lower Ca/K to one with relatively higher Ca/K (e.g., from plagioclase to pyroxene). The data show no evidence of trapped Ar and all the calculated $^{38}Ar/^{36}Ar$ have nearly a cosmogenic value of 1.54.

Cosmic-Ray Exposure (CRE) Age

The $^{38}Ar/^{36}Ar$ values for the intermediate- and high-temperature steps are indistinguishable from the cosmogenic value of 1.54. Accordingly, no correction for solar wind was made and a 2π ^{38}Ar cosmic-ray production rate of 1.090×10^{-8} cc g^{-1} Ma^{-1} was

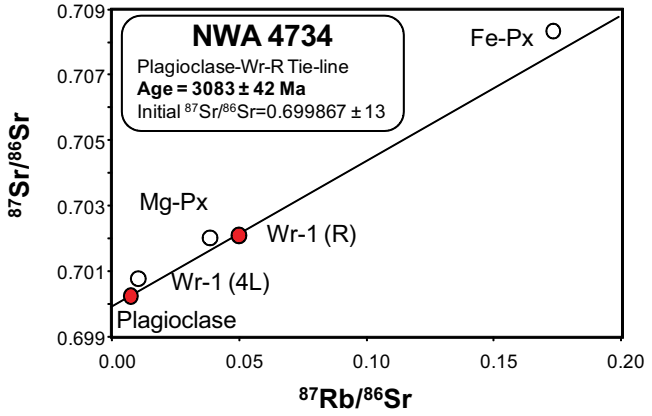


Fig. 14. Rb-Sr isochron plot of NWA 4734 mineral fractions. These data do not delineate a clear age. Scatter is interpreted to reflect addition of Sr from desert weathering. The best age of 3083 ± 42 Ma is defined by the plagioclase and WR-1 (R) fractions (red symbols). These fractions contain the most Sr (plagioclase) or were leached in the strongest reagents (Wr-1) and, consequently, are the least disturbed by the weathering process. The isochron was calculated using the IsoPlot program of Ludwig (2001) and a ^{87}Rb decay constant (λ) of 0.01402 Ga^{-1} (Begemann et al. 2001).

calculated based on the method of Eugster and Michel (1995), which takes into account the contribution from Ca, Fe, Ti, Cr, Mn, K, and Ni. For these calculations, bulk chemical composition for NWA 4734 was used and results in a CRE-age of 569 Ma for NWA 4734.

DISCUSSION

In the following discussion, we use our new data sets for NWA 4734, NWA 032, and LAP, in addition to literature data for low-Ti Apollo basalts and basaltic meteorites, to provide new insights into mantle source regions that were generating magmas at the end of the main pulse of mare magmatism. First, we examine the major element, trace element, and isotopic compositions of the three basalts to determine whether they can be reasonably interpreted as source-crater paired, as previously suggested (e.g., Zeigler et al. 2005; Wang et al. 2012). We also infer the origin of their ITE enrichment, the role (if any) of KREEP in their petrogenesis, and the composition and melting mechanisms of their mantle source region(s). Lastly, we use our data and literature data to discuss the thermal state and melting of low-Ti mare basalt source regions at approximately 2.9 Ga.

Are NWA 4734, NWA 032, and LAP 02205 Source-Crater Paired?

Despite their nearly identical Sm/Nd, Nd abundances, LREE patterns, and concordant ages, the

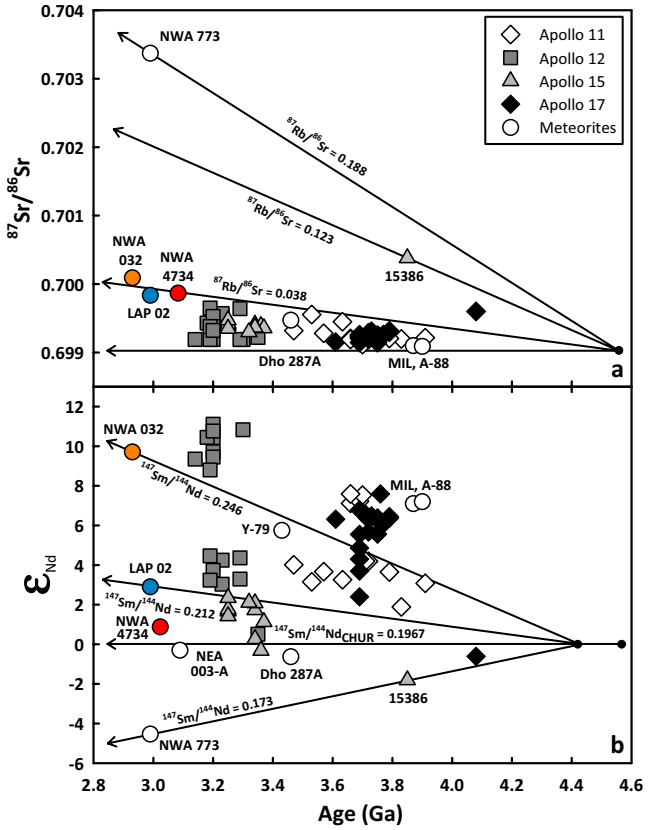


Fig. 15. Age versus initial Sr (a) and Nd (b) compositions of lunar basalts calculated from isochron analyses or whole-rock Rb-Sr and Sm-Nd isotopic systematics. The ^{87}Rb/^{86}Sr of basalt source regions are calculated assuming a single-stage model where the Moon differentiates at 4558 Ma with an initial ^{87}Sr/^{86}Sr of LUNI = 0.69903 (Nyquist et al. 1973; Nyquist 1977). The ^{147}Sm/^{144}Nd of basalt source regions are calculated assuming a two-stage model where the Moon follows a chondritic path until differentiation occurs at 4.42 Ga, at which time mare basalt source regions are formed (Nyquist and Shih 1992; Nyquist et al. 1995). Data are from numerous sources (Compston et al. 1970, 1971; Papanastassiou and Wasserburg 1970, 1973; Papanastassiou et al. 1970; Nyquist et al. 1975, 1977, 1981, 2005, 2007; Carlson and Lugmair 1979; Unruh et al. 1984; Paces et al. 1991; Shih et al. 1992, 2002; Misawa et al. 1993; Snyder et al. 1994, 1997; Torigoye-Kita et al. 1995; Borg et al. 2004; Rankenburg et al. 2006, 2007; Gaffney et al. 2007; Haloda et al. 2009).

calculated present-day source region ^{147}Sm/^{144}Nd values for NWA 032 (0.246 ± 0.004), LAP (0.212 ± 0.003), and NWA 4734 (0.201 ± 0.001) (Fig. 16) differ outside of analytical uncertainty and we argue that the three meteorites were derived from distinct source materials. However, based on their strikingly similar mineralogy, mineral chemistry, age, and bulk-rock composition, it has been suggested that they were almost certainly source-crater paired and perhaps derived from a single basaltic flow (Zeigler et al. 2005; Day and Taylor 2007; Rankenburg et al. 2007; Connolly et al. 2008;

Table 7. Summary of the constraints on the origin of NWA 032, LAP 02205, and NWA 4734.

Constraint	NWA 032	LAP 02205	NWA 4734	Supports Source-Crater Pairing Relationship?
Bulk-rock comp.	←Nearly Identical →			Yes. Although NWA 032 has minor phenocryst accumulation.
REE pattern	←Nearly Identical →			Yes.
Trace element comp.	←Nearly Identical →			Yes.
Olivine comp.	←Nearly Identical →			Yes. Not complete overlap, but consistent with different relative cooling rates.
Ni/Co in olivine	←Nearly Identical →			Yes.
Pyroxene comp.	←Nearly Identical →			Yes. Not complete overlap, but consistent with different relative cooling rates.
Pyroxene zoning	Oscillatory	Normal	Normal	Yes. NWA 4734 and LAP similar, but inconclusive for NWA 032.
Relative cooling rate	Fast	Intermediate	Slow	Yes. Consistent with a single, thick lava flow.
Crystallization Age	2931 ± 93 Ma	2991 ± 14 Ma	3024 ± 27 Ma	Yes. Ages are concordant within error.
Source $^{87}Rb/^{86}Sr$	0.044 ± 0.001	0.035 ± 0.001	0.038 ± 0.002	Yes and no. Values similar, but desert contamination obscures significance of differences.
Source $^{147}Sm/^{144}Nd$	0.246 ± 0.004	0.212 ± 0.003	0.201 ± 0.001	Yes and no. NWA 032 is an outlier. LAP and NWA 4734 similar, but well outside uncertainty.
$\varepsilon_{149}Sm$	−12.1	−3.5	−46.3	Inconclusive. Could indicate different regolith burial depths or different lava flows.
CRE-age	212–275 Ma	44 Ma	569 Ma	Inconclusive. Could indicate different regolith burial depths or different lava flows.
Lunar ejection age	47 ± 10 Ka	55 ± 5 Ka	Unknown	Yes. NWA 032 and LAP concordant within error.

See text for sources of data presented here. Source region isotopic compositions calculated using the models explained in the Fig. 15 caption.

Fernandes et al. 2009a, 2009b; Korotev et al. 2009; Wang et al. 2012). In this section, we use our new data to argue that the basalts are source-crater paired, but are unlikely to be from a single flow. A summary of the criteria that we use to assess pairing relationships is shown in Table 7.

Textures, Mineral Chemistry, and Bulk-Rock Compositions

Texturally, the sections of NWA 4734 and LAP examined here are subtly different. The differences in grain size are most apparent in pyroxene and feldspar sizes (Fig. 2), and in the large size of late-stage fayalitic olivine grains in NWA 4734 (e.g., Fig. 1d). Textural differences also relate to differences in Fe-rich pyroxene compositions in LAP (Fig. 4b) that extend completely through the "forbidden zone" toward the hedenbergite-ferrosilite join to pyroxferroite ($Ca_{0.15}Fe_{0.85}SiO_3$); a few pyroxene compositions in NWA 4734 trend toward pyroxferroite, which may indicate slower cooling rates for NWA 4734 (i.e., Lindsley and Munoz 1969; Lindsley and Burnham 1970; Lindsley et al. 1972). However, Zeigler et al. (2005) observed similar degrees of variability in grain size and pyroxene composition among subsamples of the LAP meteorites, so given our limited sample area (three thin sections of NWA 4734), it can be argued that NWA 4734 and the LAP meteorites are texturally indistinguishable. In contrast, NWA 032 is texturally dissimilar to both NWA 4734 and LAP. It contains about 17 vol% phenocryst phases in a fine-grained groundmass (Figs. 2 and 3). Nevertheless, even these stark textural differences do not preclude a pairing relationship. Day and Taylor (2007) presented a quantitative textural model wherein NWA 032 represents the chilled margin of a thick lava flow, whereas LAP (and by extension NWA 4734) represents a sample of the slowly cooled interior.

Mineral chemistry also argues for a pairing among the three basalts (Table 7). First, the phenocryst mineralogy and crystallization sequence of the three basalts is very similar (Fig. 3). Olivine, pyroxene, oxide, and plagioclase major, minor, and trace element chemistry all show considerable overlap among the three basalts (Figs. 4–7). Quadrilateral pyroxene compositions show almost complete overlap (Fig. 4), with the only differences stemming from crystallization history. The latter is particularly true for NWA 032, which was quickly cooled and therefore does not

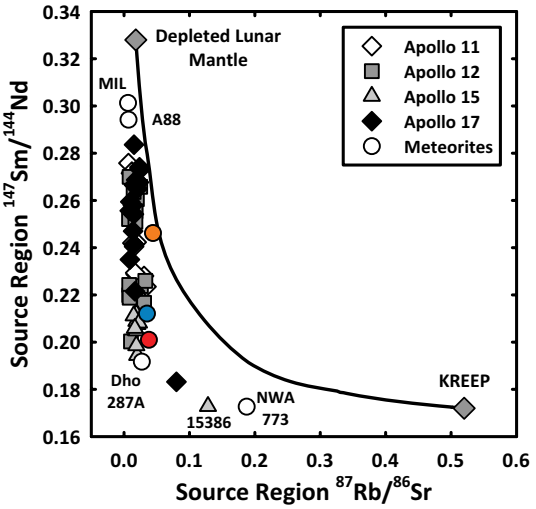


Fig. 16. Calculated present-day $^{147}Sm/^{144}Nd$ versus $^{87}Rb/^{86}Sr$ values for the source regions of lunar mare basalts using the models described in the caption of Fig. 15. The line represents a two-component mixing curve between the depleted lunar mafic cumulates estimated by Snyder et al. (1992, 1994) and the urKREEP composition of Warren and Wasson (1979). The depleted lunar mantle is estimated to have Rb = 0.05 ppm, Sr = 7.8 ppm, Sm = 0.27 ppm, Nd = 0.52 ppm, $^{87}Rb/^{86}Sr = 0.018$, and $^{147}Sm/^{144}Nd = 0.328$. The urKREEP reservoir is estimated to have Rb = 37 ppm, Sr = 200 ppm, Sm = 49 ppm, Nd = 180 ppm, $^{87}Rb/^{86}Sr = 0.52$, and $^{147}Sm/^{144}Nd = 0.172$. The source regions for NWA 4734 (red), NWA 032 (orange), and LAP (blue) show considerable spread in Sm/Nd at similar Rb/Sr.

contain pyroxene phenocrysts with more evolved compositions (Fig 4c). Pyroxene Ti/Ca drops at an Mg* of approximately 37 for both LAP and NWA 4734, indicating ilmenite saturation at virtually the same point in the crystallization sequence (Fig. 7). The Ni/Co in olivine is highly sensitive to parental magma composition (e.g., Shearer and Papike 2005; Longhi et al. 2010; Elardo et al. 2011), and suggests that the olivine in NWA 032, LAP, and NWA 4734 crystallized from parental magmas with similar Ni/Co (Fig. 5).

One clear difference between NWA 032 and LAP/NWA 4734 is distinct pyroxene zoning. Pyroxene phenocrysts in LAP and NWA 4734 display typical magmatic zoning patterns, whereas pyroxene phenocrysts in NWA 032 contain oscillatory zoning in both major and minor elements (Fig. 8). Elardo and Shearer (2014) have shown that oscillatory zoning in NWA 032 was probably the result of magma chamber convection and, possibly, injections of progressively smaller amounts of parental magma. The style and compositions of oscillatory bands also indicate that the chamber did not experience injections of a compositionally or isotopically dissimilar magma. Therefore, the LAP and NWA 4734 magmas could be derived from the same magmatic system as NWA 032, but pyroxene phenocrysts in the former two did not experience strong convection in the chamber and/or had sufficient time in the magma chamber to diffusively re-equilibrate oscillatory zoning. However, it is also suggestive that they are not derived from the same lava flow wherein NWA 032 would represent a chilled margin and NWA 4734/LAP interior regions of the flow.

The bulk-rock compositional similarities among the three meteorites extend to almost any element–element, element–ratio, or ratio–ratio plot (Figs. 10 and 11). The bulk composition of NWA 4734 from this study is nearly identical to the bulk compositions of LAP and NWA 032 (e.g., Zeigler et al. 2005; Day et al. 2006). In addition, the REE patterns of NWA 032, LAP, and NWA 4734 are parallel to subparallel and show considerable overlap (Fig. 12). Minor differences among the three basalts can probably be accounted for by mineralogic variations in sample aliquots and analytical error. The substantial compositional similarities among NWA 032, LAP, and NWA 4734 (Table 4) represent a particularly important constraint and argue strongly for a petrogenetic relationship among them.

Additional arguments can be made for a petrogenetic relationship among these three basalts when considering crystallization and ejection ages independently of isotopic compositions. NWA 4734 has a Sm-Nd age of 3024 ± 27 Ma (Fig. 13), which is concordant with the 2991 ± 14 Ma Rb-Sr age of LAP (Rankenburg et al. 2007) and the 2931 ± 92 Ma Sm-Nd age of NWA 032 (Borg et al. 2009). Ar-Ar age dating for all three rocks (e.g., Fig. S4) indicates some postcrystallization disturbance, but gives very similar ages, further supporting a petrogenetic relationship (Fernandes et al. 2003, 2009a). The CRE-age for NWA 4734 of 569 Ma is approximately 2–10× longer than the CRE-ages of 212–275 Ma for NWA 032/479 and approximately 44 Ma for LAP 02205 (Fernandes et al. 2009a), suggesting different exposure histories as rock fragments or possibly a stratigraphic relationship. In addition, Nishiizumi and Caffee (2001) and Nishiizumi et al. (2006) calculated impact ejection ages for NWA 032 and LAP, respectively, and argued that NWA 032 was ejected from the lunar surface at 47 ± 10 ka and LAP at 55 ± 5 ka (Table 7). These findings are consistent with ejection of LAP and NWA 032 in a single event.

Isotopic Compositions

The ages and initial Nd isotopic compositions determined from mineral isochrons correspond to source regions with calculated present-day $^{147}Sm/^{144}Nd$ values (assuming a two-stage model where the Moon differentiates from a chondritic reservoir at 4.42 Ga) of

0.246 ± 0.004 for NWA 032 (Borg et al. 2009), 0.212 ± 0.003 for LAP (Rankenburg et al. 2007), and 0.201 ± 0.001 for NWA 4734 (Fig. 16). These compositions indicate that NWA 032 is derived from a much more LREE-depleted source region than NWA 4734 and LAP. The difference in source region $^{147}Sm/^{144}Nd$ for NWA 4734 and LAP is smaller, but still well outside of analytical uncertainty. LAP and NWA 4734 span a similar range in initial Nd isotopic composition and calculated source region $^{147}Sm/^{144}Nd$ to the ranges observed in the Apollo basalt suites collected from single landing sites (Figs. 15 and 16). In some cases (e.g., Apollo 12 olivine basalts, Apollo 15 pigeonite basalts), those suites have been interpreted as having been derived from the same geologic units. The difference in initial Nd isotopic composition outside analytical uncertainty is, however, large enough to preclude LAP and NWA 4734 being different pieces of the same rock. Nevertheless, it is reasonable to infer, based on their overwhelming geochemical similarities, that they are probably derived from compositionally similar flows in the same volcanic province and are more than likely source-crater paired. Despite a similar geochemical similarity that includes elemental Nd, crystallization age, and lunar ejection age, the initial Nd isotopic composition of NWA 032 is so different from LAP and NWA 4734 that it precludes any simple petrogenetic relationship and leaves NWA 032 as an enigmatic outlier in the group.

Borg et al. (2009) considered analytical issues as a cause for the discrepancy in source $^{147}Sm/^{144}Nd$ between NWA 032 and LAP, but concluded that it was unlikely. No mathematical recombination of a residue–leachate pair lies on the LAP Sm-Nd isochron, and the leaching procedure used has not resulted in any isotopic fractionation in previous studies (e.g., Borg et al. 2003). The Sm-Nd spike used for the NWA 032 analyses had been recalibrated, and concurrent analyses of Martian meteorites of known age and isotopic composition yielded consistent results. Furthermore, even the smaller difference in initial Nd isotopic composition between LAP and NWA 4734 is still probably too large to attribute to differences in spike calibrations between the Lawrence Livermore and JSC labs. Consequently, Borg et al. (2009) used the LMO crystallization model of Snyder et al. (1992; Snyder Model hereafter) to model the Nd and Sr isotopic characteristics of NWA 032 and LAP source regions. These authors matched the source $^{147}Sm/^{144}Nd$ and $^{87}Rb/^{86}Sr$ values of the meteorites by using the cumulates produced during 78–95% LMO solidification, and by adding 0.1% and 0.2% urKREEP (Warren and Wasson 1979) to the source regions of NWA 032 and LAP, respectively, in addition to 2% plagioclase in the LAP source. Borg et al. (2009) estimated that NWA 032 and LAP represent approximately 2% and approximately 3.5% partial melts of their sources, respectively, based on the measured whole-rock $^{147}Sm/^{144}Nd$ and the calculated present-day ratios for their sources.

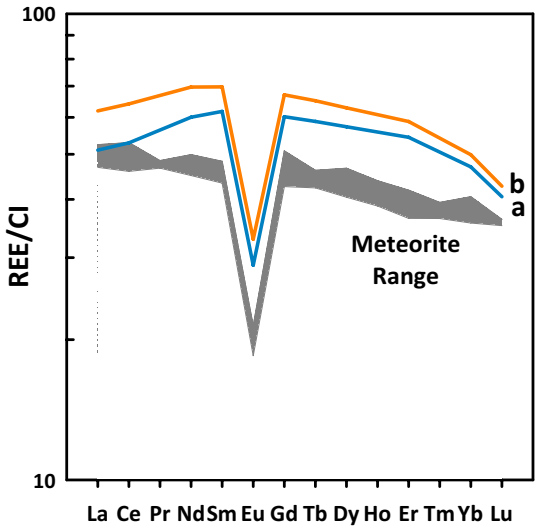


Fig. 17. Chondrite-normalized REEs patterns for the NWA 4734, NWA 032, and LAP (gray field) and equilibrium modal partial melts of the NWA 032 and LAP source regions estimated by Borg et al. (2009). REE patterns (a) represents 3.5% equilibrium modal partial melting of the Borg et al. (2009) LAP source, and REE pattern (b) represents 2% melting of the NWA 032 source; both models assume 1% trapped instantaneous residual liquid from the Snyder Model. For consistency, cumulate compositions were calculated using the estimated bulk Moon REE abundances (approximately 3× CI) from Snyder et al. (1992).

Although the Borg et al. (2009) modeled sources satisfy the isotopic constraints, they do not satisfy the geochemical constraints. In Fig. 17, we show the calculated REE patterns of 2% and 3.5% modal equilibrium partial melts of the LAP and NWA 032 source regions defined by Borg et al. (2009). We assumed 1% trapped instantaneous residual liquid (TIRL) from the Snyder Model calculations distributed among the mineral phases, and adapted the mineral/melt partition coefficients used by Snyder et al. (1992) to maintain consistency with the Borg et al. (2009) calculations. The REE patterns provide a poor fit for the observed range in NWA 4734, NWA 032, and LAP (gray field). The two calculated partial melts also show greater spread in LREE abundances (La_N = 51.0 versus 61.9) than the basalts themselves, and the calculated melts have a positive LREE slope, whereas the basalts have negative slopes. This exercise illustrates that only very minor differences in source mineralogy and trace element composition can result in noticeably different REE patterns that do not match the basalts.

It is our conclusion, based on all available data, that NWA 4734, NWA 032, and LAP cannot represent samples of the same volcanic flow. However, we conclude that they can be source-crater paired based on their overwhelming geochemical and mineralogic similarities as well as concordant crystallization and ejection ages, even though their source region isotopic characteristics are distinct. These basalts probably represent samples of temporally associated geochemically similar lava flows originating from the same volcanic complex. Their isotopic compositions indicate that either (1) multiple mantle sources were melted to feed this complex, or (2) the NWA 4734, NWA 032, and LAP parental magmas were derived from the same source, but experienced distinct assimilation histories that altered their isotopic compositions before eruption.

The Origin of Young, Low-Ti Mare Basalts NWA 4734, NWA 032, and LAP 02205

Was KREEP Involved in Their Petrogenesis?

Several authors have implicated KREEP to explain the ITE enrichment and isotopic compositions of NWA 4734, NWA 032, and LAP (Fagan et al. 2002; Righter et al. 2005; Day et al. 2006; Joy et al. 2006; Rankenburg et al. 2007; Wang et al. 2012). The issue is an important one because it has been suggested that heat from KREEP reservoirs in the lunar mantle may be needed to initiate melting over a prolonged period of time (Wieczorek and Phillips 2000; Borg et al. 2004).

Wang et al. (2012) measured the REE contents of pyroxene and plagioclase core-rim pairs in NWA 4734. The REE pattern of the melt they calculated to be in equilibrium with a plagioclase core (An_{91}) is lower in magnitude than the bulk rock, which they used to argue for assimilation of approximately 4% KREEP-rich material during basalt crystallization, but after the onset of plagioclase crystallization. However, the Wang et al. (2012) KREEP assimilation scenario is unlikely for a number of reasons. First, their measured plagioclase core-rim REE patterns are essentially parallel, which is consistent with closed-system crystal fractionation and not with assimilation of a highly LREE-enriched component. Furthermore, the REE pattern of an augite rim ($En_{12}Wo_{36}$) measured by Wang et al. (2012) has a lower LREE/HREE than the augite core ($En_{37}Wo_{29}$), which is also inconsistent with LREE-rich KREEP assimilation. Moreover, assimilation of a highly enriched (KREEPy) component after the onset of pyroxene and plagioclase crystallization would result in a disturbance of the isotopic systematics that would be reflected particularly on the Sm-Nd isochron plot (Sm-Nd being less susceptible to desert weathering than Rb-Sr). Our isotopic analyses show that two pyroxene fractions, a plagioclase fraction, and two leached whole-rock residues define an isochron with a low mean square weighted deviation (MSWD) of 1.8 (Fig. 13). If NWA 4734 assimilated a KREEPy component with a highly enriched Sm/Nd during crystallization, the whole rock should not be in isotopic equilibrium (i.e., all mineral and whole-rock fractions defining a tight isochron) with pyroxene and plagioclase fractions. Furthermore, Anand et al. (2006) and Day et al. (2006) showed that the whole-rock REE pattern for LAP is in equilibrium with the REE patterns measured in the most primitive cores of pyroxene and plagioclase, and that the core and rim REE patterns are roughly parallel. These constraints indicate no assimilation of exogenous material during basalt crystallization and little postcrystallization redistribution of REEs in those phases in LAP.

We have also investigated whether KREEP assimilation during ascent (prior to the onset of crystallization) could be responsible for range of calculated source region $^{147}Sm/^{144}Nd$ among the three basalts. NWA 032 represents the most depleted of the three basalts in terms of source $^{147}Sm/^{144}Nd$ and could represent the depleted endmember in a scenario involving progressive KREEP assimilation that leads to the more enriched source $^{147}Sm/^{144}Nd$ values for LAP and NWA 4734. In Fig. 18a, we show a two-component mixing line between NWA 032 and a KREEP endmember defined by the elemental composition of high-K KREEP (Warren 1989) and a source $^{147}Sm/^{144}Nd$ of 0.173 (from KREEPy olivine gabbro NWA 773; Borg et al. 2004, 2009). Figure 18a shows that LAP and NWA 4734 do not fall on this mixing line, indicating that their compositions cannot be derived from mixing of NWA 032 and a KREEP-rich lithology. Moreover, Fig. 18b shows the REE pattern that would result from mixing 16% high-K KREEP (assumed $^{147}Sm/^{144}Nd = 0.173$, 178 ppm Nd) and 84% NWA 032 ($^{147}Sm/^{144}Nd = 0.246$, 20.68 ppm Nd). These mixing proportions reproduce the source $^{147}Sm/^{144}Nd$ of 0.201 ± 0.001 calculated for NWA 4734 (Fig. 16); however, the REE pattern of the resulting melt demonstrates that the disparate isotopic systematics of the three basalts cannot result from mixing with KREEP without subsequently causing a great disparity in their REE patterns.

Other observations also argue against KREEP involvement in the source region of NWA 032, NWA 4734, and LAP. A relatively high $(La/Yb)_N$ of ≥ 2 and a low Ti/Sm of approximately ≤ 500 are both diagnostic features of the urKREEP reservoir that formed after extensive fractionation in the LMO (Warren and Wasson 1979). NWA 4734, NWA 032, and LAP all

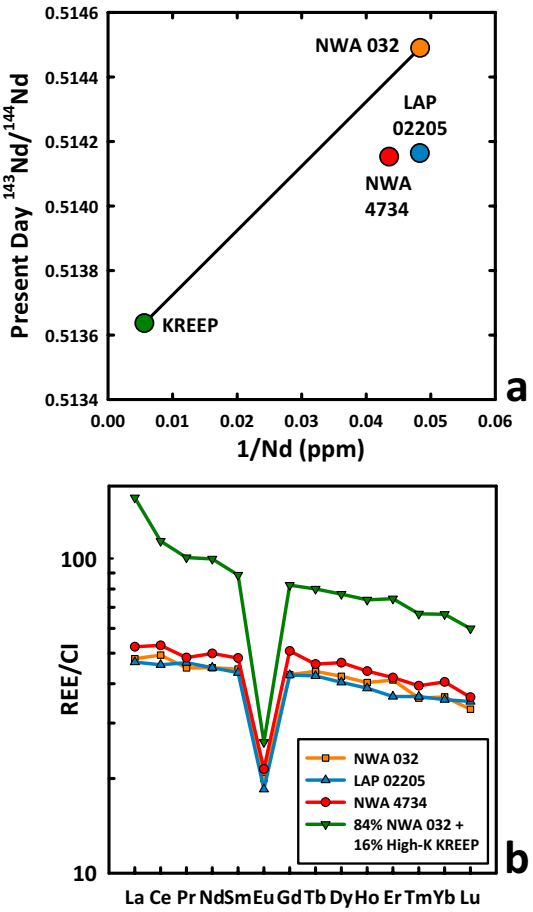


Fig. 18. (a) A two-component mixing plot of present-day $^{143}Nd/^{144}Nd$ (from leached whole-rock residue fractions) versus whole-rock 1/Nd concentrations in ppm. NWA 4734 data are from this study, NWA 032 data are from Borg et al. (2009), and LAP data are from Rankenburg et al. (2007). The KREEP endmember was estimated using the measured whole-rock $^{143}Nd/^{144}Nd$ of KREEPy olivine gabbro NWA 773 (from Borg et al. 2009) and the Nd concentration (178 ppm) of the high-K KREEP composition of Warren (1989). Two-component mixing relationships should delineate a straight line on this plot. The compositions of NWA 032, LAP, and NWA 4734 indicate that their range in source region $^{147}Sm/^{144}Nd$ cannot be derived from mixing with KREEP. (b) Chondrite-normalized REE patterns for the NWA 4734, NWA 032, LAP, and a mixture of KREEP (16%) and NWA 032 (84%). The mixture proportions reproduce the $^{147}Sm/^{144}Nd$ of the NWA 4734 source, but not its REE pattern.

have $(La/Yb)_N$ <1.5 and Ti/Sm ratios of approximately 3000, which are similar to the Apollo low-Ti basalts and not KREEP-like compositions (Fig. 11f). This argues against KREEP being responsible for the enriched trace element characteristics of the basalts.

One characteristic that could falsely be attributed to minor KREEP assimilation is the high Th content of these basalts (Figs. 11a and 11b). Wang et al. (2012) noted that a baddeleyite grain in LAP 02224 had significantly older Pb-Pb ages than sample's Sm-Nd and Rb-Sr isochron ages. If the parental magmas to these three meteorites assimilated refractory, Th-rich baddeleyite grains, then the bulk-rock compositions may be enriched in Th and give the false impression of KREEP involvement (e.g., Hui et al. 2011).

Furthermore, McCubbin et al. (2011) reported a divergence in relative abundances of magmatic volatiles (i.e., F, Cl, H) between KREEP-rich lithologies and KREEP-free mare basalts. Apatite in KREEP-rich lithologies, such as Mg- and alkali-suite rocks (e.g., troctolite 76535; McCubbin et al. 2011; Elardo et al. 2012) and KREEP-rich impact melt rocks, is typically rich in Cl and very OH-poor, whereas apatite in mare basalts typically contains extremely low Cl (<10 mole% of the X-site) and is more OH-rich. Apatite analyses from NWA 4734 and LAP (McCubbin et al. 2011) show that apatite from these basalts contain very little Cl, but are some of the most OH-rich apatites from the Moon (Fig. 9). Based on the observations of McCubbin et al. (2011), we would expect apatite in these basalts to have an elevated Cl content relative to OH if KREEP contamination occurred. These observations, in addition to the constraints from the isotopic systematics, silicate mineral chemistry, and bulk-rock trace element ratios, rule out KREEP in the source region(s) and/or assimilation of a KREEPy component as a means of producing the incompatible element enrichment in NWA 4734, LAP, and NWA 032.

Young, Incompatible Element–Enriched Lunar Basalts: Evidence for Low-Degree Partial Melting

Elevated abundances of REEs, a negatively sloping REE pattern, a deep negative Eu anomaly, and enrichment in other incompatible elements (e.g., Th) are typically interpreted as characteristics of the urKREEP reservoir (e.g., Warren 1989). However, based on the evidence presented above, KREEP was probably not involved in the petrogenesis of NWA 032, LAP, and NWA 4734. This inference and the young ages of these basalts become important for identifying heat sources for mantle melting late in lunar history after the Moon had cooled significantly, as well as for understanding mechanisms of incompatible element enrichment. Snyder et al. (1997) suggested that the relative differences in initial Nd isotopic composition between the young, isotopically depleted, KREEP-free Apollo 12 ilmenite and olivine/pigeonite basalts were related to the amount of TIRL from the LMO in their source regions. NWA 4734 and LAP have lower source region $^{147}Sm/^{144}Nd$ values than the Apollo 12 suites and are enriched in ITEs; therefore, these basalts may represent low-degree partial melts of source regions that contained approximately the same amount of, or

slightly more, TIRL than, for example, the Apollo 12 olivine/pigeonite source regions, and perhaps crystallized from a later stage liquid in the LMO.

To assess whether this is viable, we have conducted partial melting calculations on model LMO cumulate compositions. For these calculations, we used the Snyder Model of LMO crystallization, as this model (albeit simplified) is widely used by workers investigating partial melting of the lunar mantle. The starting LMO REE abundances for this set of calculations are adopted from Warren (2005), who presented his best estimate for the REE abundances for the bulk Moon. Our modeled cumulate packages and partial melts do not include urKREEP. Figure 19 illustrates our results with the chondrite-normalized REE patterns of 1% modal equilibrium partial melts of the mantle cumulate horizons produced from 78–86% LMO solidification (pattern a; ol:pig = 53:47), 86–95% LMO solidification (pattern c; pig:cpx = 41:59), and a 50–50 mixture of the two (pattern b; ol:pig:cpx = 27:44:30). All cumulates contained 1% TIRL from the LMO distributed among the mineral phases (for comparison, Snyder et al. [1997] suggested 0.3–0.5% TIRL for the Apollo 12 olivine/pigeonite basalt source). The REE pattern of a 1% partial melt of the cumulates formed between 86 and 95% LMO solidification (pattern c in Fig. 19) has a $(La/Yb)_N$ of 1.48, a $(La/Sm)_N$ of 1.08, and a Eu/Eu* of 0.50. This is similar to NWA 4734, NWA 032, and LAP, with $(La/Yb)_N$ of 1.29–1.32, $(La/Sm)_N$ of 1.08–1.09, and Eu/Eu* of 0.43–0.46. A similar REE pattern in the partial melt of this LMO cumulate package can also be reproduced by inclusion of 0–5% TIRL and assuming 0.1–5% partial melting; however, in large cumulate piles (i.e., 100–1000 m thick piles in Earth's gravitational field), gravitationally driven compaction can result in filter pressing and the expulsion of intercumulus melt down to <1% (e.g., Sparks et al. 1985). Therefore, the inclusion of more than approximately 1% TIRL in LMO cumulates is probably not justified. Furthermore, low-degree partial melts of more primitive cumulates are also LREE-enriched (e.g., pattern a in Fig. 19), and would become more similar to the meteoritic basalts if they underwent fractional crystallization before eruption, as suggested by Day et al. (2006); however, accounting for a deep negative Eu anomaly is problematic in this scenario. As the isotopic compositions of these basalts should reflect the compositions of the source regions, these LREE-enriched melts should still have depleted Nd isotopic compositions reflecting long-term depletion in Sm/Nd in their source regions.

This modeling demonstrates that using a reasonable model of LMO crystallization, some TIRL, and low degrees of partial melting, basalts with KREEP-like trace element characteristics can be produced by normal petrologic processes without the need to invoke contamination from urKREEP material. It is not, however, meant to suggest that the mantle cumulates derived from 86–95% crystallization in the Snyder model are the only possible source materials for NWA 4734, NWA 032, and LAP. The numerous degrees of freedom in this type of modeling (e.g., starting LMO composition, cumulate line of descent, amount and composition of TIRL, degree and nature of mixing during cumulate overturn, degree of partial melting, choice of partition coefficients) preclude such specific arguments from being made.

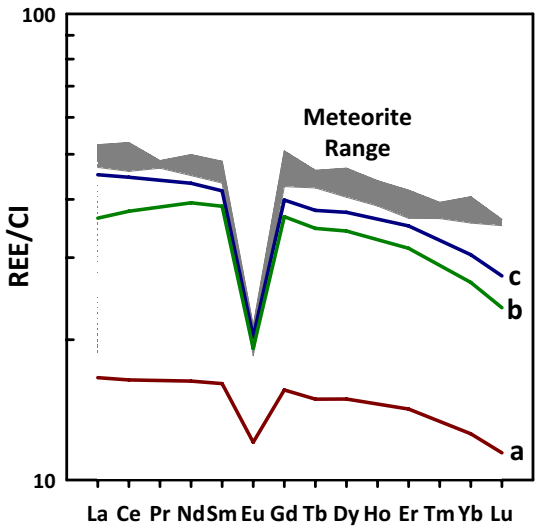


Fig. 19. Chondrite-normalized REE patterns for NWA 4734, NWA 032, and LAP (gray field) with 1% equilibrium modal partial melts of the LMO cumulates produced during 78–86% crystallization (pattern a; ol:pig = 53:47), 86–95% crystallization (pattern c; pig:cpx = 41:59), and a 50:50 mixture of the two (pattern b; ol:pig:cpx = 27:44:30), and from the Snyder Model. Cumulate compositions were calculated using the estimated bulk Moon REE abundances (approximately 2.4× CI) from Warren (2005) and assuming 1% trapped instantaneous residual liquid. CI chondrite composition is that of Lodders and Fegley (1998; and references within).

It is possible that these basalts represent magmas that have undergone extensive fractional crystallization before eruption (e.g., Day et al. 2006); however, based on our trace element modeling of source region melting, this is not required and would not account for the deep negative Eu anomaly. Without the involvement of KREEP, a deep Eu/Eu* must be inherited from the source region (olivine and low-Ca pyroxene fractionation will not appreciably deepen the Eu anomaly), or from the presence of plagioclase in the residuum after partial melting, the latter of which seems

unlikely, given low alumina content (<10 wt%) of these three basalts. Cumulate source regions with similar Eu/Eu* crystallize from the LMO between approximately 90–95% solid in the Snyder Model. This inference would be consistent with the low Mg*s and elevated ITE abundances expected in later stage LMO cumulates. Bulk compositions with a low Ni/Co and low absolute abundances of Ni and Co would also be expected for a basalt derived from a more evolved cumulate source (Shearer et al. 1996, 2006), which is consistent with observations of the three basalts (Fig. 11e). Three basalts represent liquid compositions and potentially low-degree partial melts of an Fe-rich source region formed late during LMO crystallization; this suggests that they would be good candidates for experimental work to better constrain the mineralogy of their source regions (e.g., presence or absence of plagioclase) and the average temperatures and depths of melting.

Basaltic Lunar Meteorites and Low-Ti Mare Volcanism on the Moon

The ten unbrecciated basaltic lunar meteorites discovered thus far have significantly expanded our knowledge of the compositional and isotopic variability in lunar mantle source regions that have produced low-Ti mare basalts, as well as the time period over which melting occurred (Misawa et al. 1993; Torigoye-Kita et al. 1995; Fagan et al. 2003; Jolliff et al. 2003; Borg et al. 2004, 2009; Rankenburg et al. 2007; Gaffney et al. 2008; Joy et al. 2008; Sokol et al. 2008; Terada et al. 2008; Haloda et al. 2009; Liu et al. 2009). When considering the information they provide as well as the data from previous studies of the Apollo low-Ti basalt suites (e.g., Shervais et al. 1990; Neal et al. 1994a, 1994b; Snyder et al. 1997, 2000; Beard et al. 1998; Neal 2001; Ryder and Schuraytz 2001, among others), we can make a number of important general observations about low-Ti mare magmatism on the Moon.

First, the production of low- and very low-Ti mare magmas represents, by far, the most voluminous type of volcanism on the Moon (Giguere et al. 2000; Gillis et al. 2003) and was a long-lived process, occurring for more than 1 Gyr of lunar history. The basalt clast in Kalahari 009 bounds the older end of this range at 4.30 Ga (Terada et al. 2007; Shih et al. 2008; Sokol et al. 2008) and NWA 032 the younger end at 2.93 Ga (Borg et al. 2009). Second, low-Ti mare magmas from multiple Apollo landing sites and basaltic meteorites often exhibit significant compositional overlap in major (e.g., Al versus Mg) and minor/trace elements (e.g., Th versus Sm; Figs. 10 and 11). However, differences in TiO_2, Mg*, REE patterns (Fig. 12), and various other trace elements and trace element ratios (e.g., Neal et al. 1994b) demonstrate that there is significant compositional diversity in low-Ti sources throughout the lunar mantle. Third, the isotopic diversity observed among low-Ti mare basalts and their inferred source regions is significant, implying that low-Ti magmas were being produced from multiple source regions throughout lunar history. Calculated $^{147}Sm/^{144}Nd$ values for low-Ti sources span a considerable range from 0.294 for Asuka-881757 (Misawa et al. 1993) to 0.173 for NWA 773 (Borg et al. 2004, 2009). This range essentially spans the entire range of values calculated for all lunar magma source regions. The range in geochemical and isotopic compositions in young lunar basalts indicates that there are multiple mechanisms for producing KREEP-like incompatible element–enriched lunar magmas (i.e., Borg et al. 2009).

Finally, the compositional and isotopic variability of the youngest basalts provides insight into the thermal state of the mantle at approximately 2.9–3.0 Ga. NWA 4734, NWA 032, and LAP are basalts that do not appear to have been affected by KREEP. Their incompatible element–enriched compositions are consistent with low-degree partial melting of later stage LMO cumulates with lower solidus temperatures than the more Mg-rich source regions of at least some older low-Ti basalts. Although KREEP may be a source of heat for partial melting at approximately 2.9 Ga, melting may not always occur where KREEP resides in the mantle (i.e., Borg et al. 2004). NWA 773, however, is a basaltic cumulate with a similarly young age of 2.99 Ga (Borg et al. 2009) that is clearly connected to KREEP (Fig. 15), indicating that both heat and mass from KREEP were involved in the production of some young mare basalts. Conversely, the low-Ti mare basaltic meteorite NEA 003A is the same age (3.09 Ga) within error as NWA 4734, NWA 773, and LAP, but has a higher Mg* (53), low abundances of ITEs (Haloda et al. 2009), and a source region $^{147}Sm/^{144}Nd$ that is essentially chondritic (0.195) and consistent with its REE pattern (Fig. 12). As such, NEA 003A indicates that, at approximately 3 Ga, the lunar mantle melted to simultaneously generate both ITE-enriched, low-Mg* basalts as well as ITE-depleted, higher Mg* basalts, some of which have very similar source region isotopic compositions. The significant range in geochemical and isotopic compositions demonstrates that melting in the lunar mantle at the end of the main pulse of mare magmatism cannot be simply linked to KREEP involvement or fertility of the source region; it is probably a complex process that requires further study, as well as additional samples, to understand completely.

SUMMARY

We have conducted an integrated petrologic, mineralogic, geochemical, and isotopic study of lunar basaltic meteorites NWA 4734, NWA 032, and LAP 02205 with the goals of (1) determining if they are crater-paired and (2) placing better constraints on the magmatic processes involved in the petrogenesis of the youngest known mare basalts. Our main conclusions and interpretations based on this study are:

- NWA 4734 is a low-Ti mare basalt that is very similar to NWA 032 and LAP. These three basalts show considerable overlap in bulk-rock major, minor, and trace element compositions, mineral compositions, Ni/Co in olivine, as well as ejection and crystallization ages, despite some textural differences. They are more than likely source-crater paired. However, their calculated source region $^{147}Sm/^{144}Nd$ values are different outside of analytical uncertainty and suggest that they are derived from different lava flows from the same volcanic complex on the Moon.
- Despite elevated abundances of incompatible trace elements and a deep negative Eu anomaly, KREEP was not involved in the petrogenesis of these three basalts. This conclusion is based on high bulk-rock Ti/Sm, similar $(La/Yb)_N$ to other KREEP-poor low-Ti basalts, Cl-poor apatite compositions, and isotopic equilibrium between minerals and the bulk rock. Also, the range in source region $^{147}Sm/^{144}Nd$ values cannot be derived from mixing of the isotopically depleted NWA 032 composition with KREEP. Rather, model partial melting calculations suggest that their deep negative Eu anomalies and LREE-enriched compositions are more consistent with low-degree partial melting of relatively Fe-rich, but KREEP-free late-stage LMO cumulates.
- The geochemical characteristics that are typically attributed to urKREEP are not unique to that reservoir (also see Borg et al. 2009). Basalts with KREEP-like geochemical characteristics, such as a deep negative Eu anomaly and a high LREE/HREE, can be generated within the lunar mantle by normal petrologic processes, such as low-degree partial melting, or by melting of a late-stage LMO cumulate source. Such source regions, if they include even small amounts (i.e., ≤1%) of trapped melt, should have trace element characteristics similar to KREEP. Invocation of the presence of KREEP in a mantle source region or of its assimilation by an ascending magma requires more evidence than a deep negative Eu anomaly, a negatively sloping REE pattern, and slightly elevated ITE abundances.
- Combining the data presented here with literature data for similarly young low-Ti meteorites NWA 773 (KREEPy) and NEA 003A, it becomes apparent that melting in the lunar mantle at the end of the main pulse of mare magmatism was occurring contemporaneously in multiple source regions with very different geochemical and isotopic characteristics. This is probably a reflection of varying heat sources, and therefore the most recent mantle melting cannot be attributed solely to straightforward explanations, such as heat from KREEP in the mantle.

Acknowledgments—We thank Tony Irving and Stefan Ralew for kindly providing samples of NWA 4734 for isotopic analyses, Mike Spilde for assistance with thin section scale WDS mapping, Tim Teague for sample mounting, Kent Ross for assistance during EMPA work for Ar-Ar analyses, Tim Becker for keeping the mass spectrometers at BGC healthy, the Meteorite Working Group at NASA JSC for allocating us samples of the LAP meteorites, the IOM Meteorite Collection for samples of NWA 4734, and Jim Papike and James Day for many helpful discussions. We also thank Ryan Zeigler and an anonymous reviewer for comments that substantively improved this manuscript, and Randy Korotev for his work and comments as AE. This work was funded by NASA Earth and Space Science Fellowship NNX12AO15H to S.M.E. and NASA Cosmochemistry grants NNX10AI77G to C.K.S. and NNX09AB92G to C.R.N. A portion of this work was performed under the auspices of the U.S. D.O.E. by Lawrence Livermore National Laboratory under contract DE-AC52-07NA27344. F.M.M. acknowledges support from Lunar Advanced Science and Exploration Research (LASER) grant NNX13AK32G, and V.A.F. acknowledges support from the Ann and Gordon Getty Foundation while a Postdoctoral Research Fellow at the BGC. In addition, S.M.E. gratefully acknowledges support from a graduate fellowship from the NM Space Grant Consortium. This research has made use of NASA's Astrophysics Data System.

Editorial Handling—Dr. Randy Korotev

REFERENCES

Anand M., Taylor L. A., Misra K. C., Demidova S. I., and Nazarov M. A. 2003. KREEPy lunar meteorite Dhofar 287A: A new lunar mare basalt. *Meteoritics & Planetary Science* 38:485–499.

Anand M., Taylor L. A., Floss C., Neal C. R., Terada K., and Tanikawa S. 2006. Petrology and geochemistry of

LaPaz Icefield 02205: A new unique low-Ti mare-basalt meteorite. *Geochimica et Cosmochimica Acta* 70:246–264.

Barrat J. A., Chaussidon M., Bohn M., Gillet P., Gopel C., and Lesourd M. 2005. Lithium behavior during cooling of a dry basalt: An ion-microprobe study of the lunar meteorite Northwest Africa 479 (NWA 479). *Geochimica et Cosmochimica Acta* 69:5597–5609.

Beard B. L., Taylor L. A., Scherer E. E., Johnson C. M., and Snyder G. A. 1998. The source region and melting mineralogy of high-titanium and low-titanium lunar basalts deduced from Lu-Hf isotope data. *Geochimica et Cosmochimica Acta* 62:525–544.

Begemann F., Ludwig K. R., Lugmair G. W., Min K., Nyquist L. E., Patchett P. J., Renne P. R., Shih C. Y., Villa I. M., and Walker R. J. 2001. Call for an improved set of decay constants for geochronological use. *Geochimica et Cosmochimica Acta* 65:111–121.

Bence A. E. and Papike J. J. 1972. Pyroxenes as recorders of lunar basalt petrogenesis: Chemical trends due to crystal-liquid interaction. *Geochimica et Cosmochimica Acta* 3:431–469.

Borg L. E., Nyquist L. E., Reese Y., and Wiesmann H. 2003. The age of Dar al Gani 476 and the differentiation history of the martian meteorites inferred from their Rb-Sr, Sm-Nd, and Lu-Hf isotopic systematics. *Geochimica et Cosmochimica Acta* 67:3519–3536.

Borg L. E., Shearer C. K., Asmerom Y., and Papike J. J. 2004. Prolonged KREEP magmatism on the Moon indicated by the youngest dated lunar igneous rock. *Nature* 432:209–211.

Borg L. E., Gaffney A. M., Shearer C. K., DePaolo D. J., Hutcheon I. D., Owens T. L., Ramon E., and Brennecka G. 2009. Mechanisms for incompatible element enrichment on the Moon deduced from the lunar basaltic meteorite Northwest Africa 032. *Geochimica et Cosmochimica Acta* 73:3963–3980.

Bouchet M., Kaplan G., Voudon A., and Bertoletti M. J. 1971. Spark mass spectrometric analysis of major and minor elements in six lunar samples. *Geochimica et Cosmochimica Acta* 2:1247–1252.

Brunfelt A. O., Heier K. S., and Steinnes E. 1971. Determination of 40 elements in Apollo 12 materials by neutron activation analysis. *Geochimica et Cosmochimica Acta* 2:1281–1290.

Brunfelt A. O., Heier K. S., Nilssen B., Steinnes E., and Sundvoll B. 1972. Elemental composition of Apollo 15 samples. In *The Apollo 15 lunar samples*, pp. 195–197.

Burger P. V., Shearer C. K., and Papike J. J. 2009. The multi-stage cooling history of lunar meteorite NWA 032 as recorded by phenocrystic olivine and pyroxene (abstract #2043). 40th Lunar and Planetary Science Conference. CD-ROM.

Burgess R. and Turner G. 1998. Laser ^{40}Ar-^{39}Ar age determinations of Luna 24 mare basalts. *Meteoritics & Planetary Science* 33:921–935.

Carlson R. W. and Lugmair G. W. 1979. Sm-Nd constraints on early lunar differentiation and the evolution of Kreep. *Earth and Planetary Science Letters* 45:123–132.

Chappell B. W. and Green D. H. 1973. Chemical compositions and petrogenetic relationships in Apollo 15 mare basalts. *Earth and Planetary Science Letters* 18:237–246.

Compston W., Chappell B. W., Arriens P. A., and Vernon M. J. 1970. The chemistry and age of Apollo 11 lunar material. Proceedings, Apollo 11 Lunar Science Conference. pp. 1007–1027.

Compston W., Berry H., Vernon M. J., Chappell B. W., and Kaye M. J. 1971. Rubidium-strontium chronology and chemistry of lunar material from the Ocean of Storms. *Geochimica et Cosmochimica Acta* 2:1471–1485.

Compston W., De Laeter J. R., and Vernon M. J. 1972. Strontium isotope geochemistry of Apollo 15 basalts. In *The Apollo 15 lunar samples*, pp. 347–351.

Connolly H. C., Smith C., Benedix G., Folco L., Righter K., Zipfel J., Yamaguchi A., and Aoudjehane H. C. 2008. The Meteoritical Bulletin, No. 93. *Meteoritics & Planetary Science* 43:571–632.

Cuttitta F., Rose H. J. Jr., Annell C. S., Carron M. K., Christian R. P., Dwornik E. J., Greenland L. P., Helz A. W., and Ligon D. T. Jr. 1971. Elemental composition of some Apollo 12 lunar rocks and soils. *Geochimica et Cosmochimica Acta* 2:1217–1229.

Cuttitta F., Rose H. J. Jr., Annell C. S., Carron M. K., Christian R. P., Dwornik E. J., and Ligon D. T. Jr. 1973. Compositional study of twenty-one Apollo 15 lunar rocks and soils. Proceedings, 4th Lunar Science Conference. pp. 167–168.

Day J. M. D. and Taylor L. A. 2007. On the structure of mare basalt lava flows from textural analysis of the LaPaz Icefield and Northwest Africa 032 lunar meteorites. *Meteoritics & Planetary Science* 42:3–17.

Day J. M. D., Taylor L. A., Floss C., Patchen A. D., Schnare D. W., and Pearson D. G. 2006. Comparative petrology, geochemistry, and petrogenesis of evolved, low-Ti lunar mare basalt meteorites from the LaPaz ice field, Antarctica. *Geochimica et Cosmochimica Acta* 70:1581–1600.

Duncan A. R., Sher M. K., Abraham Y. C., Erlank A. J., Willis J. P., and Ahrens L. H. 1975. Compositional variability of the Apollo 15 regolith. Proceedings, 7th Lunar Science Conference. pp. 220–222.

Elangovan P., Hezel D. C., Howard L., Armstrong R., and Abel R. L. 2012. PhaseQuant: A tool for quantifying tomographic data sets of geological specimens. *Computers & Geosciences* 48:323–329.

Elardo S. M. and Shearer C. K. 2014. Magma chamber dynamics recorded by oscillatory zoning in pyroxene and olivine phenocrysts in basaltic lunar meteorite Northwest Africa 032. *American Mineralogist*, doi:10.2138/am.2014.4552.

Elardo S. M., Draper D. S., and Shearer C. K. 2011. Lunar Magma Ocean crystallization revisited: Bulk composition, early cumulate mineralogy, and the source regions of the highlands Mg-suite. *Geochimica et Cosmochimica Acta* 75:3024–3045.

Elardo S. M., McCubbin F. M., and Shearer C. K. 2012. Chromite symplectites in Mg-suite troctolite 76535 as evidence for infiltration metasomatism of a lunar layered intrusion. *Geochimica et Cosmochimica Acta* 87:154–177.

Engel A. E. J., Engel C. G., Sutton A. L., and Myers A. T. 1971. Composition of five Apollo 11 and Apollo 12 rocks and one Apollo 11 soil and some petrogenic considerations. *Geochimica et Cosmochimica Acta* 2:439–448.

Eugster O. and Michel T. 1995. Common asteroid break-up events of eucrites, diogenites, and howardites and cosmic-ray production-rates for noble-gases in achondrites. *Geochimica et Cosmochimica Acta* 59:177–199.

Fagan T. J., Taylor G. J., Keil K., Bunch T. E., Wittke J. H., Korotev R. L., Jolliff B. L., Gillis J. J., Haskin L. A., Jarosewich E., Clayton R. N., Mayeda T. K., Fernandes V. A., Burgess R., Turner G., Eugster O., and Lorenzetti S. 2002. Northwest Africa 032: Product of lunar volcanism. *Meteoritics & Planetary Science* 37:371–394.

Fagan T. J., Taylor G. J., Keil K., Hicks T. L., Killgore M., Bunch T. E., Wittke J. H., Mittlefehldt D. W., Clayton R. N., Mayeda T. K., Eugster O., Lorenzetti S., and Norman M. D. 2003. Northwest Africa 773: Lunar origin and iron-enrichment trend. *Meteoritics & Planetary Science* 38:529–554.

Fernandes V. A. and Burgess R. 2005. Volcanism in mare fecunditatis and mare crisium: Ar-Ar age studies. *Geochimica et Cosmochimica Acta* 69:4919–4934.

Fernandes V. A., Burgess R., and Turner G. 2000. Laser ^{40}Ar-^{39}Ar age studies of Dar al Gani 262 lunar meteorite. *Meteoritics & Planetary Science* 35:1355–1364.

Fernandes V. A., Burgess R., and Turner G. 2003. ^{40}Ar-^{39}Ar chronology of lunar meteorites Northwest Africa 032 and 773. *Meteoritics & Planetary Science* 38:555–564.

Fernandes V. A., Burgess R., and Morris A. 2009a. ^{40}Ar-^{39}Ar age determinations of lunar basalt meteorites Asuka 881757, Yamato 793169, Miller Range 05035, La Paz Icefield 02205, Northwest Africa 479, and basaltic breccia Elephant Moraine 96008. *Meteoritics & Planetary Science* 44:805–821.

Fernandes V. A., Korotev R. L., and Renne P. R. 2009b. ^{40}Ar-^{39}Ar ages and chemical composition for lunar mare basalts: NWA 4734 and NWA 4898 (abstract #1045). 40th Lunar and Planetary Science Conference. CD-ROM.

Flanagan F. J. 1984. Three USGS mafic rock reference samples, W-2, DNC-1, and BIR-1. *U.S. Geological Survey Bulletin* 1623:54.

Fletcher I. R. and Rosman K. J. R. 1982. Precise determination of initial $_{Nd}$ from Sm-Nd isochron data. *Geochimica et Cosmochimica Acta* 46:1983–1987.

Fruchter J. S., Stoeser J. W., Lindstrom M. M., and Goles G. G. 1973. Apollo 15 clastic materials and their relationship to local geologic features. *Geochimica et Cosmochimica Acta* 2(Suppl. 4):1227–1237.

Gaffney A. M., Borg L. E., and Asmerom Y. 2007. The origin of geochemical diversity of lunar mantle sources inferred from the combined U-Pb, Rb-Sr, and Sm-Nd isotope systematics of mare basalt 10017. *Geochimica et Cosmochimica Acta* 71:3656–3671.

Gaffney A. M., Borg L. E., DePaolo D. J., and Irving A. J. 2008. Age and isotope systematics of Northwest Africa 4898, a new type of highly-depleted mare basalt (abstract #1877). 39th Lunar and Planetary Science Conference. CD-ROM.

Ganapathy R., Morgan J. W., Krahenbuhl U., and Anders E. 1973. Ancient meteoritic components in lunar highland rocks: Clues from trace elements in Apollo 15 and 16 samples. *Geochimica et Cosmochimica Acta* 2(Suppl. 4):1239–1261.

Giguere T. A., Taylor G. J., Hawke B. R., and Lucey P. G. 2000. The titanium contents of lunar mare basalts. *Meteoritics & Planetary Science* 35:193–200.

Gillis J. J., Jolliff B. L., and Elphic R. C. 2003. A revised algorithm for calculating TiO_2 from Clementine UVVIS data: A synthesis of rock, soil, and remotely sensed TiO_2 concentrations. *Journal of Geophysical Research: Planets* (1991–2012), 108:E2.

Gladney E. S. and Roelandts I. 1988. 1987 compilation of elemental concentration data for USGS BIR-1, DNC-1 and W-2. *Geostandards Newsletter* 12:63–118.

Goldoff B., Webster J. D., and Harlov D. E. 2012. Characterization of fluor-chlorapatites by electron probe microanalysis with a focus on time-dependent intensity variation of halogens. *American Mineralogist* 97:1103–1115.

Govindaraju K. 1994. 1994 compilation of working values and sample description for 383 geostandards. *Geostandards Newsletter* 18:1–158.

Greshake A., Irving A. J., Kuehner S. M., Korotev R. L., Gellissen M., and Palme H. 2008. Northwest Africa 4898: A new high-alumina mare basalt from the Moon (abstract #1631). 39th Lunar and Planetary Science Conference. CD-ROM.

Haloda J., Tycova P., Korotev R. L., Fernandes V. A., Burgess R., Thoni M., Jelenc M., Jakes P., Gabzdyl P., and Kosler J. 2009. Petrology, geochemistry, and age of low-Ti mare-basalt meteorite Northeast Africa 003-A: A possible member of the Apollo 15 mare basaltic suite. *Geochimica et Cosmochimica Acta* 73:3450–3470.

Haskin L. A., Helmke P. A., Allen R. O., Anderson M. R., Korotev R. L., and Zweifel K. A. 1971. Rare-earth elements in Apollo 12 lunar materials. *Geochimica et Cosmochimica Acta* 2:1307–1317.

Helmke P. A., Blanchard D. P., Haskin L. A., Telander K., Weiss C., and Jacobs J. W. 1973. Major and trace elements in igneous rocks from Apollo 15. *The Moon* 8:129–148.

Hess P. C. and Parmentier E. M. 2001. Thermal evolution of a thicker KREEP liquid layer. *Journal of Geophysical Research-Planets* 106:28,023–28,032.

Hiesinger H., Jaumann R., Neukum G., and Head J. W. 2000. Ages of mare basalts on the lunar nearside. *Journal of Geophysical Research-Planets* 105:29,239–29,275.

Hiesinger H., Head J. W., Wolf U., Jaumann R., and Neukum G. 2003. Ages and stratigraphy of mare basalts in Oceanus Procellarum, Mare Nubium, Mare Cognitum, and Mare Insularum. *Journal of Geophysical Research: Planets* (1991–2012), 108:E7.

Hiesinger H., Head III J. W., Wolf U., Jaumann R., and Neukum G. 2010. Ages and stratigraphy of lunar mare basalts in Mare Frigoris and other nearside maria based on crater size-frequency distribution measurements. *Journal of Geophysical Research* 115:E03003.

Hill E., Taylor L. A., Floss C., and Liu Y. 2009. Lunar meteorite LaPaz Icefield 04841: Petrology, texture, and impact-shock effects of a low-Ti mare basalt. *Meteoritics & Planetary Science* 44:87–94.

Hubbard N. J. and Gast P. W. 1971. Chemical composition and origin of nonmare lunar basalts. *Geochimica et Cosmochimica Acta* 2:999–1020.

Hui H. J., Oshrin J. G., and Neal C. R. 2011. Investigation into the petrogenesis of Apollo 14 high-Al basaltic melts through crystal stratigraphy of plagioclase. *Geochimica et Cosmochimica Acta* 75:6439–6460.

Jenner G. A., Longerich H. P., Jackson S. E., and Fryer B. J. 1990. ICP-MS: A powerful tool for high-precision trace-element analysis in Earth sciences: Evidence from analysis of selected USGS reference samples. *Chemical Geology* 83:133–148.

Jolliff B. L., Korotev R. L., Zeigler R. A., and Floss C. 2003. Northwest Africa 773: Lunar mare breccia with a shallow-

formed olivine-cumulate component, inferred very-low-Ti (VLT) heritage, and a KREEP connection. *Geochimica et Cosmochimica Acta* 67:4857–4879.

Joy K. H., Crawford I. A., Downes H., Russell S. S., and Kearsley A. T. 2006. A petrological, mineralogical, and chemical analysis of the lunar mare basalt meteorite LaPaz Icefield 02205, 02224, and 02226. *Meteoritics & Planetary Science* 41:1003–1025.

Joy K. H., Crawford I. A., Anand M., Greenwood R. C., Franchi I. A., and Russell S. S. 2008. The petrology and geochemistry of Miller Range 05035: A new lunar gabbroic meteorite. *Geochimica et Cosmochimica Acta* 72:3822–3844.

Karner J., Papike J. J., and Shearer C. K. 2003. Olivine from planetary basalts: Chemical signatures that indicate planetary parentage and those that record igneous setting and process. *American Mineralogist* 88:806–816.

Koeberl C., Kurat G., and Brandstaetter F. 1993. Gabbroic lunar mare meteorites Asuka-881757 (Asuka-31) and Yamato-793169: Geochemical and mineralogical study. *Proceedings of the NIPR Symposium on Antarctic Meteorites* 6:14–34.

Korotev R. L. 2005. Lunar geochemistry as told by lunar meteorites. *Chemie Der Erde-Geochemistry* 65:297–346.

Korotev R. L., Jolliff B. L., Zeigler R. A., Gillis J. J., and Haskin L. A. 2003. Feldspathic lunar meteorites and their implications for compositional remote sensing of the lunar surface and the composition of the lunar crust. *Geochimica et Cosmochimica Acta* 67:4895–4923.

Korotev R. L., Zeigler R. A., Irving A. J., and Bunch T. E. 2009. Keeping up with the lunar meteorites–2009 (abstract #1137). 40th Lunar and Planetary Science Conference. CD-ROM.

Kushiro I. and Haramura H. 1971. Major element variation and possible source materials of Apollo 12 crystalline rocks. *Science* 171:1235–1237.

Lindsley D. H. and Burnham C. W. 1970. Pyroxferroite: Stability and X-ray crystallography of synthetic $Ca_{0.15}Fe_{0.85}SiO_3$ pyroxenoid. *Science* 168:364–367.

Lindsley D. H., and Munoz J. L. 1969. Subsolidus relations along the join hedenbergite-ferrosilite. *American Journal of Science*, 267-A:295–324.

Lindsley D. H., Papike J. J., and Bence A. E. 1972. Pyroxferroite: Breakdown at low pressure and high temperature. Proceedings, 3rd Lunar Science Conference. pp. 483–485.

Liu Y., Floss C., Day J. M. D., Hill E., and Taylor L. A. 2009. Petrogenesis of lunar mare basalt meteorite Miller Range 05035. *Meteoritics & Planetary Science* 44:261–284.

Lodders K. and Fegley B. 1998. *The planetary scientist's companion*. New York: Oxford University Press. pp. xvii, 371.

Longhi J., Durand S. R., and Walker D. 2010. The pattern of Ni and Co abundances in lunar olivines. *Geochimica et Cosmochimica Acta* 74:784–798.

Lucey P., Korotev R. L., Gillis J. J., Taylor L. A., Lawrence D., Campbell B. A., Elphic R., Feldman B., Hood L. L., Hunten D., Mendillo M., Noble S., Papike J. J., Reedy R. C., Lawson S., Prettyman T., Gasnault O., and Maurice S. 2006. Understanding the lunar surface and space-moon interactions. In *Reviews in Mineralogy and Geochemistry*, edited by Jolliff B. L., Wieczorek M. A., Shearer C. K., and Neal C. R. Washington, D.C.: Mineralogical Society of America. pp. 83–219.

Ludwig K. R. 2001. *Users manual for Isoplot/Ex v. 2.49: A geochronological toolkit for microsoft excel*. Berkeley, California: Berkeley Geochronology Center Special Publication No. 1a.

Mahoney J. J., Fitton J. G., Wallace P. J., and Coffin M. 2001. Basement drilling of the Ontong 600 Java Plateau: Covering Leg 192 of the cruises of the Drilling Vessel "Joides Resolution," 601 Apra Harbour, Guam, to Apra Harbor, Guam, sites 1183-1187, 8 September-7 November 602 2000. In *Proceedings of the Ocean Drilling Program, Initial Reports*, 75 pp. College Station, Texas: Texas A & M University Ocean Drilling Program.

Mason B., Jarosewich E., and Melson W. G. 1972. Mineralogy, petrology, and chemical composition of lunar samples 15085, 15256, 15271, 15471, 15475, 15476, 15535, 15555, and 15556. *Geochimica et Cosmochimica Acta* 3:785–796.

Maxwell J. A. and Wiik H. B. 1971. Chemical composition of Apollo 12 lunar samples 12004, 12033, 12051, 12052 and 12065. *Earth and Planetary Science Letters* 10:285–288.

McCubbin F. M., Steele A., Hauri E. H., Nekvasil H., Yamashita S., and Hemley R. J. 2010a. Nominally hydrous magmatism on the Moon. *Proceedings of the National Academy of Sciences* 107:11,223–11,228.

McCubbin F. M., Steele A., Nekvasil H., Schnieders A., Rose T., Fries M., Carpenter P. K., and Jolliff B. L. 2010b. Detection of structurally bound hydroxyl in fluorapatite from Apollo mare basalt 15058,128 using TOF-SIMS. *American Mineralogist* 95:1141–1150.

McCubbin F. M., Jolliff B. J., Nekvasil H., Carpenter P. K., Zeigler R. A., Steele A., Elardo S. M., and Lindsley D. H. 2011. Fluorine and chlorine abundances in lunar apatite: Implications for heterogeneous distributions of magmatic volatiles in the lunar interior. *Geochimica et Cosmochimica Acta* 75:5073–5093.

Misawa K., Tatsumoto M., Dalrymple G. B., and Yanai K. 1993. An extremely low U/Pb source in the Moon: U-Th-Pb, Sm-Nd, Rb-Sr, and Ar-40 Ar-39 isotopic systematics and age of lunar meteorite Asuka 881757. *Geochimica et Cosmochimica Acta* 57:4687–4702.

Neal C. R. 2001. Interior of the Moon: The presence of garnet in the primitive deep lunar mantle. *Journal of Geophysical Research* 106:27,865–27,885.

Neal C. R. and Kramer G. Y. 2003. The composition of KREEP: A detailed study of KREEP basalt 15386 (abstract #2023). 34th Lunar and Planetary Science Conference. CD-ROM.

Neal C. R. and Taylor L. A. 1992. Petrogenesis of mare basalts: A record of lunar volcanism. *Geochimica et Cosmochimica Acta* 56:2177–2211.

Neal C. R., Hacker M. D., Snyder G. A., Taylor L. A., Liu Y.-G., and Schmitt R. A. 1994a. Basalt generation at the Apollo 12 site: Part 1, New data, classification, and re-evaluation. *Meteoritics* 29:334–348.

Neal C. R., Hacker M. D., Snyder G. A., Taylor L. A., Liu Y.-G., and Schmitt R. A. 1994b. Basalt generation at the Apollo 12 site: Part 2, Source heterogeneity, multiple melts, and crustal contamination. *Meteoritics* 29:349–361.

Nishiizumi K. and Caffee M. W. 2001. Exposure histories of lunar meteorites Northwest Africa 032 and Dhofar 081 (abstract #2101). 32nd Lunar and Planetary Science Conference. CD-ROM.

Nishiizumi K., Hillegonds D. J., and Welten K. C. 2006. Exposure and terrestrial histories of lunar meteorites LAP 02205/02224/02226/02436, MET 01210, and PCA 02007 (abstract #2369). 37th Lunar and Planetary Science Conference. CD-ROM.

Nyquist L. E. 1977. Lunar Rb-Sr chronology. *Physics and Chemistry of the Earth* 10:103–142.

Nyquist L. E. and Shih C. Y. 1992. The isotopic record of lunar volcanism. *Geochimica et Cosmochimica Acta* 56:2213–2234.

Nyquist L. E., Hubbard N. J., Gast P. W., Bansal B. M., Wiesmann H., and Jahn B. 1973. Rb-Sr systematics for chemically defined Apollo 15 and 16 materials. *Geochimica et Cosmochimica Acta* 2(Suppl. 4):1823–1846.

Nyquist L. E., Bansal B. M., and Wiesmann H. 1975. Rb-Sr ages and initial $^{87}Sr/^{86}Sr$ for Apollo 17 basalts and KREEP basalt 15386. Proceedings, 6th Lunar Science Conference. pp. 1445–1465.

Nyquist L. E., Bansal B. M., Wooden J. L., and Wiesmann H. 1977. Sr-isotopic constraints on the petrogenesis of Apollo 12 mare basalts. Proceedings 8th Lunar Science Conference. pp. 1383–1415.

Nyquist L. E., Wooden J. L., Shih C. Y., Wiesmann H., and Bansal B. M. 1981. Isotopic and REE studies of lunar basalt 12038: Implications for petrogenesis of aluminous mare basalts. *Earth and Planetary Science Letters* 55:335–355.

Nyquist L. E., Wiesmann H., Bansal B., Shih C. Y., Keith J. E., and Harper C. L. 1995. ^{146}Sm-^{142}Nd formation interval for the lunar mantle. *Geochimica et Cosmochimica Acta* 59:2817–2837.

Nyquist L. E., Shih C. Y., Reese Y., and Bogard D. D. 2005. Age of lunar meteorite LAP02205 and implications for impact-sampling of planetary surfaces (abstract #1347). 36th Lunar and Planetary Science Conference. CD-ROM.

Nyquist L. E., Shih C. Y., and Reese Y. D. 2007. Sm-Nd and Rb-Sr ages for MIL 05035: Implications for surface and mantle sources (abstract #1702). 38th Lunar and Planetary Science Conference. CD-ROM.

O'Kelley G. D., Eldridge J. S., Northcutt K. J., and Schonfeld E. 1972. Primordial radioelements and cosmogenic radionuclides in lunar samples from Apollo 15. *Geochimica et Cosmochimica Acta* 3:1659–1670.

Paces J. B., Nakai S., Neal C. R., Taylor L. A., Halliday A. N., and Lee D. C. 1991. A strontium and neodymium isotopic study of Apollo 17 high-Ti mare basalts: Resolution of ages, evolution of magmas, and origins of source heterogeneities. *Geochimica et Cosmochimica Acta* 55:2025–2043.

Papanastassiou D. A. and Wasserburg G. J. 1970. Rb-Sr ages from the Ocean of storms. *Earth and Planetary Science Letters* 8:269–278.

Papanastassiou D. A. and Wasserburg G. J. 1973. Rb-Sr ages and initial strontium in basalts from Apollo 15. *Earth and Planetary Science Letters* 17:324–337.

Papanastassiou D. A., Wasserburg G. J., and Burnett D. S. 1970. Rb-Sr ages of lunar rocks from the sea of tranquillity. *Earth and Planetary Science Letters* 8:1–19.

Papike J. J., Ryder G., and Shearer C. K. 1998. Lunar samples. In *Planetary materials*, edited by Papike J. J. Reviews in Mineralogy, vol. 36. Washington, D.C.: Mineralogical Society of America. pp. 5-1–5-234.

Papike J. J., Fowler G. W., Adcock C. T., and Shearer C. K. 1999. Systematics of Ni and Co in olivine from planetary melt systems: Lunar mare basalts. *American Mineralogist* 84:392–399.

Pyle J. M., Spear F. S., and Wark D. A. 2002. Electron microprobe analysis of REE in apatite, monazite and xenotime: Protocols and pitfalls. *Phosphates: Geochemical, Geobiological, and Materials Importance* 48:337–362.

Rankenburg K., Brandon A. D., and Neal C. R. 2006. Neodymium isotope evidence for a chondritic composition of the Moon. *Science* 312:1369–1372.

Rankenburg K., Brandon A. D., and Norman M. D. 2007. A Rb-Sr and Sm-Nd isotope geochronology and trace element study of lunar meteorite LaPaz Icefield 02205. *Geochimica et Cosmochimica Acta* 71:2120–2135.

Renne P. R., Swisher C. C., Deino A. L., Karner D. B., Owens T. L., and DePaolo D. J. 1998. Intercalibration of standards, absolute ages and uncertainties in ^{40}Ar-^{39}Ar dating. *Chemical Geology* 145:117–152.

Rhodes J. M. and Hubbard N. J. 1973. Chemistry, classification, and petrogenesis of Apollo 15 mare basalts. Proceedings, 4th Lunar Science Conference. pp. 1127–1148.

Rhodes J. M., Blanchard D. P., Dungan M. A., Brannon J. C., and Rodgers K. V. 1977. Chemistry of Apollo 12 mare basalts: Magma types and fractionation processes. Proceedings, 8th Lunar Science Conference. pp. 1305–1338.

Righter K., Collins S. J., and Brandon A. D. 2005. Mineralogy and petrology of the LaPaz Icefield lunar mare basaltic meteorites. *Meteoritics & Planetary Science* 40:1703–1722.

Russ G. P., Burnett D. S., Lingenfelter R. E., and Wasserburg G. J. 1971. Neutron capture on ^{149}Sm in lunar samples. *Earth and Planetary Science Letters* 13:53–60.

Ryder G. and Schuraytz B. C. 2001. Chemical variation of the large Apollo 15 olivine-normative mare basalt rock samples. *Journal of Geophysical Research-Planets* 106:1435–1451.

Shearer C. K. and Papike J. J. 1999. Magmatic evolution of the Moon. *American Mineralogist* 84:1469–1494.

Shearer C. K. and Papike J. J. 2005. Early crustal building processes on the Moon: Models for the petrogenesis of the magnesian suite. *Geochimica et Cosmochimica Acta* 69:3445–3461.

Shearer C. K., Papike J. J., and Layne G. D. 1996. Deciphering basaltic magmatism on the Moon from the compositional variations in the Apollo 15 very low-Ti picritic magmas. *Geochimica et Cosmochimica Acta* 60:509–528.

Shearer C. K., Hess P. C., Wieczorek M. A., Pritchard M. E., Parmentier E. M., Borg L. E., Longhi J., Elkins-Tanton L. T., Neal C. R., Antonenko I., Canup R. M., Halliday A. N., Grove T. L., Hager B. H., Lee D. C., Wiechert U., and Jolliff B. L. 2006. Thermal and magmatic evolution of the Moon. In *New views of the Moon*, edited by Jolliff B. L., Wieczorek M. A., Shearer C. K., and Neal C. R. Reviews in Mineralogy and Geochemistry, vol. 60. Washington, D.C.: Mineralogical Society of America. pp. 365–518.

Shervais J. W., Vetter S. K., and Lindstrom M. M. 1990. Chemical differences between small subsamples of Apollo 15 olivine-normative basalts. Proceedings, 20th Lunar and Planetary Science Conference. pp. 109–126.

Shih C. Y., Nyquist L. E., Bansal B. M., and Wiesmann H. 1992. Rb-Sr and Sm-Nd chronology of an Apollo 17 Kreep basalt. *Earth and Planetary Science Letters* 108:203–215.

Shih C. Y., Nyquist L. E., Reese Y., Wiesmann H., Nazarov M. A., and Taylor L. A. 2002. The chronology and petrogenesis of the mare basalt clast from lunar meteorite

Dhofar 287: Rb-Sr and Sm-Nd isotopic studies (abstract 1344). 33rd Lunar and Planetary Science Conference. CD-ROM.

Shih C. Y., Nyquist L. E., Reese Y., and Bischoff A. 2008. Sm-Nd and Rb-Sr isotopic studies of meteorite Kalahari 009: An old VLT mare basalt (abstract #2165). 39th Lunar and Planetary Science Conference. CD-ROM.

Snyder G. A., Taylor L. A., and Neal C. R. 1992. A chemical model for generating the sources of mare basalts: Combined equilibrium and fractional crystallization of the lunar magmasphere. *Geochimica et Cosmochimica Acta* 56:3809–3823.

Snyder G. A., Lee D.-C., Taylor L. A., Halliday A. N., and Jerde E. A. 1994. Evolution of the upper mantle of the Earth's Moon: Neodymium and strontium isotopic constraints from high-Ti mare basalts. *Geochimica et Cosmochimica Acta* 58:4795–4808.

Snyder G. A., Neal C. R., Taylor L. A., and Halliday A. N. 1997. Anatexis of lunar cumulate mantle in time and space: Clues from trace-element, strontium, and neodymium isotopic chemistry of parental Apollo 12 basalts. *Geochimica et Cosmochimica Acta* 61:2731–2747.

Snyder G. A., Borg L. E., Nyquist L. E., and Taylor L. A. 2000. Chronology and isotopic constraints on lunar evolution. In *Origin of the Earth and Moon*, edited by Canup R. M. and Righter K. Tucson, Arizona: The University of Arizona Press. pp. 361–395.

Sokol A. K., Fernandes V. A., Schulz T., Bischoff A., Burgess R., Clayton R. N., Munker C., Nishiizumi K., Palme H., Schultz L., Weckwerth G., Mezger K., and Horstmann M. 2008. Geochemistry, petrology and ages of the lunar meteorites Kalahari 008 and 009: New constraints on early lunar evolution. *Geochimica et Cosmochimica Acta* 72:4845–4873.

Sparks R. S. J., Huppert H. E., Kerr R. C., Mckenzie D. P., and Tait S. R. 1985. Postcumulus processes in layered intrusions. *Geological Magazine* 122:555–568.

Steiger R. H. and Jäger E. 1977. Subcommission on geochronology: Convention on use of decay constants in geochronology and cosmochronology. *Earth and Planetary Science Letters* 36:359–362.

Stormer J. C., Pierson M. L., and Tacker R. C. 1993. Variation of F-X-Ray and Cl-X-Ray intensity due to anisotropic diffusion in apatite during electron-microprobe analysis. *American Mineralogist* 78:641–648.

Taylor S. R., Rudowski R., Muir P., Graham A., and Kaye M. 1971. Trace element chemistry of lunar samples from the Ocean of Storms. *Geochimica et Cosmochimica Acta* 2:1083–1099.

Terada K., Anand M., Sokol A. K., Bischoff A., and Sano Y. 2007. Cryptomare magmatism 4.35 Gyr ago recorded in lunar meteorite Kalahari 009. *Nature* 450:849–852.

Terada K., Sasaki Y., Anand M., Sano Y., Taylor L. A., and Horie K. 2008. Uranium-lead systematics of low-Ti basaltic meteorite Dhofar 287A: Affinity to Apollo 15 green glasses. *Earth and Planetary Science Letters* 270:119–124.

Torigoye-Kita N., Misawa K., Dalrymple G. B., and Tatsumoto M. 1995. Further evidence for a low U/Pb source in the Moon: U-Th-Pb, Sm-Nd, and Ar-Ar isotopic systematics of lunar meteorite Yamato 793169. *Geochimica et Cosmochimica Acta* 59:2621–2632.

Turner G. 1971. ^{40}Ar-^{39}Ar dating: Optimization of irradiation parameters. *Earth and Planetary Science Letters* 10:227–234.

Unruh D. M., Stille P., Patchett P. J., and Tatsumoto M. 1984. Lu-Hf and Sm-Nd evolution in lunar mare basalts. *Journal of Geophysical Research* 89(Suppl. B):459–477.

Wang Y., Hsu W., Guan Y., Li X., Li Q., Liu Y., and Tang G. 2012. Petrogenesis of the Northwest Africa 4734 basaltic lunar meteorite. *Geochimica et Cosmochimica Acta* 92:329–344.

Wänke H., Wlotzka F., Baddenhausen H., Balacescu A., Spettel B., Teschke F., Jagoutz E., Kruse H., Quijano-Rico M., and Rieder R. 1971. Apollo 12 samples: Chemical composition and its relation to sample locations and exposure ages, the two component origin of the various soil samples and studies on lunar metallic particles. *Geochimica et Cosmochimica Acta* 2:1187–1208.

Wänke H., Palme H., Baddenhausen H., Dreibus G., Jagoutz E., Kruse H., Palme C., Spettel B., Teschke F., and Thacker R. 1975. New data on the chemistry of lunar samples: Primary matter in the lunar highlands and the bulk composition of the Moon. Proceedings, 6th Lunar Science Conference. pp. 1313–1340.

Wänke H., Palme H., Kruse H., Baddenhausen H., Cendales M., Dreibus G., Hofmeister H., Jagoutz E., Palme C., Spettel B., and Thacker R. 1976 Chemistry of lunar highland rocks: A refined evaluation of the composition of the primary matter. Proceedings, 7th Lunar Science Conference. pp. 3479–3499.

Warren P. H. 1989. KREEP: Major-element diversity, trace-element uniformity (almost). *Workshop on the Moon in Transition: Apollo 14, KREEP and Evolved Lunar Rocks* 89-03, pp. 149–153.

Warren P. H. 2005. "New" lunar meteorites: Implications for composition of the global lunar surface, lunar crust, and bulk Moon. *Meteoritics & Planetary Science* 40:477–506.

Warren P. H. and Wasson J. T. 1979. Origin of KREEP. *Reviews of Geophysics and Space Physics* 17:73–88.

Warren P. H., Shirley D. N., and Kallemeyn G. W. 1986. A potpourri of pristine Moon rocks, including a VHK mare basalt and a unique, augite-rich Apollo 17 anorthosite. *Journal of Geophysical Research* 91:D319–D330.

Wieczorek M. A. and Phillips R. J. 2000. The "Procellarum KREEP Terrane": Implications for mare volcanism and lunar evolution. *Journal of Geophysical Research* 105:20,417–20,430.

Willis J. P., Ahrens L. H., Danchin R. V., Erlank A. J., Gurney J. J., Hofmeyr P. K., McCarthy T. S., and Orren M. J. 1971. Some interelement relationships between lunar rocks and fines, and stony meteorites. *Geochimica et Cosmochimica Acta* 2:1123–1138.

Willis J. P., Erlank A. J., Gurney J. J., Theil R. H., and Ahrens L. H. 1972. Major, minor, and trace element data for some Apollo 11, 12, 14, and 15 samples. *Geochimica et Cosmochimica Acta* 3:1269–1273.

Yanai K. and Kojima H. 1991. Varieties of lunar meteorites recovered from Antarctica. *Proceedings of the NIPR Symposium on Antarctic Meteorites* 4:70–90.

Zeigler R. A., Korotev R. L., Jolliff B. L., and Haskin L. A. 2005. Petrography and geochemistry of the LaPaz Icefield basaltic lunar meteorite and source crater pairing with Northwest Africa 032. *Meteoritics & Planetary Science* 40:1073–1101.

SUPPORTING INFORMATION

Additional supporting information may be found in the online version of this article:

Fig S1: Mineral separations procedure for Sm-Nd and Rb-Sr isotopic analyses.

Fig S2: Compositions of Fe-Ti-Cr-oxides in NWA 4734, 032, and LAP 02205/224.

Fig S3: Compositions of plagioclase in NWA 4734 and LAP 02205/224.

Fig S4: Ar-Ar age spectrums from step-heating for NWA 4734.

Table S1: Standard reference materials data for ICP-MS and –OES analyses of NWA 4734.

Table S2: EMP analyses of olivine in NWA 4734, 032, and LAP 02205/224.

Table S3: SIMS analyses of Ni and Co in olivine in NWA 4734, 032, and LAP 02205/224.

Table S4: EMP analyses of Fe-Ti-Cr-oxides in NWA 4734, 032, and LAP 02205/224.

Table S5: EMP analyses of pyroxene in NWA 4734, 032, and LAP 02205/224.

Table S6: EMP analyses of plagioclase in NWA 4734, 032, and LAP 02205/224.

Table S7: EMP analyses of phosphates in NWA 4734.

Table S8: Ar-Ar step-heating data.